Cellular/Molecular

APOE4 Affects Basal and NMDAR-Mediated Protein Synthesis in Neurons by Perturbing Calcium Homeostasis

Sarayu Ramakrishna,[1,2,7] Vishwaja Jhaveri,[1] Sabine C. Konings,[3] Bharti Nawalpuri,[1,6,7] Sumita Chakraborty,[1] Bjørn Holst,[4] Benjamin Schmid,[4] Gunnar K. Gouras,[3] Kristine K. Freude,[5] and Ravi S. Muddashetty[1,7]

[1]Institute for Stem Cell Science and Regenerative Medicine, Bangalore 560065, India, [2]The University of Trans-Disciplinary Health Sciences and Technology (TDU), Bangalore 560064, India, [3]Experimental Dementia Research Unit, Department of Experimental Medical Science, Lund University, Lund 22184, Sweden, [4]Bioneer A/S, Hørsholm 2970, Denmark, [5]Department of Veterinary and Animal Sciences, Group of Stem Cell Models for Studies of Neurodegenerative Diseases, Section for Pathobiological Sciences, Faculty of Health and Medical Sciences, University of Copenhagen, Denmark, [6]The Shanmugha Arts, Science, Technology and Research Academy, Thanjavur 613401, India, and [7]Centre for Brain Research, Indian Institute of Science Campus, Bangalore 560012, India

Apolipoprotein E (APOE), one of the primary lipoproteins in the brain has three isoforms in humans, APOE2, APOE3, and APOE4. APOE4 is the most well-established risk factor increasing the predisposition for Alzheimer's disease (AD). The presence of the APOE4 allele alone is shown to cause synaptic defects in neurons and recent studies have identified multiple pathways directly influenced by APOE4. However, the mechanisms underlying APOE4-induced synaptic dysfunction remain elusive. Here, we report that the acute exposure of primary cortical neurons or synaptoneurosomes to APOE4 leads to a significant decrease in global protein synthesis. Primary cortical neurons were derived from male and female embryos of Sprague Dawley (SD) rats or C57BL/6J mice. Synaptoneurosomes were prepared from P30 male SD rats. APOE4 treatment also abrogates the NMDA-mediated translation response indicating an alteration of synaptic signaling. Importantly, we demonstrate that both APOE3 and APOE4 generate a distinct translation response which is closely linked to their respective calcium signature. Acute exposure of neurons to APOE3 causes a short burst of calcium through NMDA receptors (NMDARs) leading to an initial decrease in protein synthesis which quickly recovers. Contrarily, APOE4 leads to a sustained increase in calcium levels by activating both NMDARs and L-type voltage-gated calcium channels (L-VGCCs), thereby causing sustained translation inhibition through eukaryotic translation elongation factor 2 (eEF2) phosphorylation, which in turn disrupts the NMDAR response. Thus, we show that APOE4 affects basal and activity-mediated protein synthesis responses in neurons by affecting calcium homeostasis.

Key words: **Alzheimer's disease; APOE; calcium; L-VGCC; NMDAR; protein synthesis**

Significance Statement

Defective protein synthesis has been shown as an early defect in familial Alzheimer's disease (AD). However, this has not been studied in the context of sporadic AD, which constitutes the majority of cases. In our study, we show that Apolipoprotein E4 (APOE4), the predominant risk factor for AD, inhibits global protein synthesis in neurons. APOE4 also affects NMDA activity-mediated protein synthesis response, thus inhibiting synaptic translation. We also show that the defective protein synthesis mediated by APOE4 is closely linked to the perturbation of calcium homeostasis caused by APOE4 in neurons. Thus, we propose the dysregulation of protein synthesis as one of the possible molecular mechanisms to explain APOE4-mediated synaptic and cognitive defects. Hence, the study not only suggests an explanation for the APOE4-mediated predisposition to AD, it also bridges the gap in understanding APOE4-mediated pathology.

Received Mar. 2, 2021; revised Aug. 15, 2021; accepted Aug. 22, 2021.

Author contributions: S.R., S.C.K., G.K.G., K.K.F., and R.S.M. designed research; S.R., V.J., S.C.K., B.N., S.C., and R.S.M. performed research; B.H., B.S., G.K.G., K.K.F., and R.S.M. contributed unpublished reagents/analytic tools; S.R., V.J., S.C.K., and S.C. analyzed data; S.R. and R.S.M. wrote the first draft of the paper; S.R., G.K.G., K.K.F., and R.S.M. edited the paper; S.R. and R.S.M. wrote the paper.

This work was supported by the NeuroStem Grant BT/IN/Denmark/07/RSM/2015-2016. S.R. was supported by the Junior/Senior Research Fellowship DBT/2016/InStem/540 from the Department of Biotechnology (DBT). G.K.G. was supported by the EU H2020 Marie Sklodowska–Curie Grant 721802 (SYNDEGEN) and the Swedish Research Council Grant 2019-01125. S.C.K. was supported by the EU H2020 Marie Sklodowska–Curie Grant 721802 (SYNDEGEN). We thank all the central facilities at NCBS-inStem, especially the Central Imaging and Flow Cytometry Facility (CIFF), Animal House Facility, and Stem Cell Facility; our collaborators and colleagues for their invaluable suggestions and discussions; specially Dr. Sumantra Chattarji and his lab members from National Center for Biological Sciences, Bangalore, for all the technical help and conceptual scientific discussions; Dr. James Chelliah from JNCASR, Bangalore, for giving us MK801; and thank Dr. Vijayalakshmi Ravindranath and Dr. Reddy P. Kommaddi from Centre for Brain Research, Bangalore, for their generous gift of MAP2 antibody and B27 during the revision experiments.

The authors declare no competing financial interests.

Correspondence should be addressed to Ravi S. Muddashetty at ravism@instem.res.in or ravimshetty@iisc.ac.in.

https://doi.org/10.1523/JNEUROSCI.0435-21.2021

Copyright © 2021 the authors

Introduction

Alzheimer's disease (AD) is an irreversible progressive neurodegenerative disorder that leads to loss of memory and cognition (Hardy, 2006). Pathologically, AD is characterized by brain atrophy along with accumulation of Aβ plaques and neurofibrillary tangles (Hardy, 2006). But, the most robust correlation for the severity of dementia and staging of AD is with the extent of synapse loss, which occurs presymptomatically (Shankar and Walsh, 2009). The maintenance and re-modeling of synapses requires the synthesis of new proteins which are tightly regulated spatiotemporally (Kelleher et al., 2004; Sutton and Schuman, 2006). Thus, activity mediated synthesis of new proteins and changes in the proteome play an important role in driving synaptic plasticity (Kelleher et al., 2004; Sutton and Schuman, 2006; Suzanne Zukin et al., 2009).

Multiple studies have shown the dysregulation of protein synthesis and its machinery in AD. Alterations in the amount, activity, and posttranslational modifications of translation components like eukaryotic translation initiation factor 2 subunit α (eIF2α), eukaryotic translation elongation factor 1α1 (eEF1A), eukaryotic translation initiation factor 4E (eIF4E), and p70 ribosomal protein S6 (RPS6) kinase 1 are reported (An et al., 2003; Li et al., 2004; Ma et al., 2010; Beckelman et al., 2016; Yang et al., 2016). Intriguingly, altered expression of rRNA and mRNAs coding for ribosomal proteins are documented to occur presymptomatically in AD (Ding et al., 2005, 2006; Hernández-Ortega et al., 2016). Accordingly, studies have revealed a dysregulation of de-novo protein synthesis in AD (Cefaliello et al., 2020; Elder et al., 2021) as well as in other forms of taupathies (Moreno et al., 2013; Radford et al., 2015; Meier et al., 2016; Evans et al., 2019; Koren et al., 2019). Along with basal translation, defects in synaptic activity mediated signaling and translation is also reported to occur presymptomatically in AD (Ma et al., 2010; Yang et al., 2016; Ahmad et al., 2017; Cefaliello et al., 2020). However, the link between defective translation and dysregulation of synaptic signaling is not explored, and is likely to be an important early event in AD pathology.

Apart from the familial mutations which occur in only 10% of the population, many genetic factors which significantly increase the risk of AD have been identified (Tanzi, 2012). Apolipoprotein isoform ε4 (APOE4) is the most well-established genetic risk factor for AD which increases the frequency of occurrence and decreases the age of onset significantly (Kim et al., 2009; Liu et al., 2013). APOE4, unlike the other isoforms APOE2 and APOE3, is shown to increase the predisposition to AD by affecting the clearance of Aβ (Kim et al., 2009; Liu et al., 2013). However, many studies have reported that the presence of APOE4 allele can cause synaptic defects independently. Reduction of neurite outgrowth, dendritic complexity, spine density, and loss of synaptic proteins is well reported in APOE4 mouse models (Nathan et al., 1994; Teter et al., 2002; Dumanis et al., 2009; Rodriguez et al., 2013; Yong et al., 2014). Consequently, APOE4 mice of both younger and older age groups are reported to show defects in spatial learning and memory (Rodriguez et al., 2013). Further evidence comes from studies drawing correlations between the APOE genotype and cognitive impairment in humans (Small et al., 2004; Wisdom et al., 2011; De Jager et al., 2012; Reas et al., 2019). Moreover, APOE4 is reported to interfere with the glutamate receptor signaling pathways (Chen et al., 2010), particularly with NMDA receptors (NMDARs; Bacskai et al., 2000; Sheng et al., 2008; Nakajima et al., 2013), indicating that APOE receptors are present as a part of the postsynaptic density (PSD) complex (May et al., 2004). Thus, APOE activates multiple signaling pathways in neurons with key signaling differences between the APOE isoforms (Hoe et al., 2005; Huang et al., 2017, 2019).

Although APOE4 is indicated to be one of the key factors influencing synaptic loss and cognitive defects in AD, the molecular mechanisms behind this are still unclear. Here, we show that APOE4 inhibits basal and NMDAR-mediated protein synthesis by increasing eukaryotic translation elongation factor 2 (eEF2) phosphorylation. APOE4-mediated translation response is linked to the increased calcium influx caused by activation of NMDARs and L-type voltage-gated calcium channels (L-VGCCs). Thus, the dysregulation of calcium homeostasis by APOE4 leads to its impaired protein synthesis response.

Materials and Methods

Ethics statement

All animal work was conducted in accordance with the procedures approved by the Institutional Animal Ethics Committee (IAEC) and the Institutional Biosafety Committee (IBSC), InStem, Bangalore, India. All rodent work was done with Sprague Dawley (SD) rats. Rats were kept in 20–22 °C temperature, 50–60 relative humidity, 0.3-μm high-efficiency particulate air (HEPA)-filtered air supplied at 15–20 ACPH, and 14 h/10 h light/dark cycle maintained.

All the human stem cell work was conducted in accordance with and approval from the Institutional Human Ethics Committee, Institutional Stem Cell Committee, and Institutional Biosafety Committee at InStem, Bangalore, India.

Rat primary neuronal cultures

Primary neuronal cultures were prepared from cerebral cortices of SD rat embryos [embryonic day (E)18.5] as previously published by our lab (Kute et al., 2019; Ravindran et al., 2019; Ghosh Dastidar et al., 2020). Briefly, the cortex tissue was trypsinized and homogenized using 0.25% trypsin. The dissociated cells were plated on precoated poly-L-lysine (P2636, Sigma) dishes at a density of 40,000–50,000 cells/cm^2 for biochemistry experiments and 30,000–40,000 cells/cm^2 for imaging-based experiments. The plates were coated with poly-L-lysine solution (0.2 mg/ml) made in borate buffer (pH 8.5) for 5–6 h and excess solution was washed with water. For imaging experiments, the neurons were plated on nitric acid-treated coverslips which were coated with poly-L-lysine. For all the experiments, the neurons were initially plated on MEM (10095080, ThermoFisher Scientific) supplemented with 10% fetal bovine serum (FBS) to aid their attachment. After 3 h in MEM, the media was changed to Neurobasal (21103049, ThermoFisher Scientific) supplemented with B27 (17504044, ThermoFisher Scientific) and 1× Glutamax. The neurons were maintained in culture for 15–20 d at 37°C, 5% CO_2 conditions by supplementing Neurobasal media every 5–6 d.

Induced pluripotent stem cell (iPSC) maintenance and conditioned media collection

The iPSCs [APOE knock-out (KO), APOE 3/3, and APOE 4/4] were obtained from Bioneer A/S. Briefly, the iPSCs from an 18-year-old male of APOE 3/4 genotype were subjected to clustered regularly interspaced short palindromic repeats (CRISPR)-Caspase 9 (Cas9) gene editing to obtain isogenic iPSC lines of APOE KO, APOE 3/3, and APOE 4/4 genotypes (Schmid et al., 2019). The iPSCs were maintained in mTeSR1 complete media (72 232, Stem Cell Technologies) at 37°C, 5% CO_2 conditions. A mixture of 1-mg/ml Collagenase IV (17104019, ThermoFisher Scientific), 0.25% Trypsin, 20% KO serum (10828028, ThermoFisher Scientific), 1 mM calcium chloride (made in PBS) was used to dissociate the iPSCs for passaging.

Once the iPSCs reached ~50% confluency, the media was changed from mTeSR1 to Neurobasal + Glutamax. The iPSCs were maintained in Neurobasal-based media for 48 h. After 48 h, the conditioned media were given a short spin at 1000 × g for 2 min to remove the cell debris

and subjected to ELISA (ab108813, Abcam) to estimate the amount of APOE secreted by iPSCs.

Synaptoneurosome preparation

Synaptoneurosomes were prepared from cortices of postnatal day (P)30 male SD rats as previously published (Muddashetty et al., 2007; Kute et al., 2019; Paul et al., 2019). Briefly, cortices were homogenized at 4°C in 10 volumes of the synaptoneurosome buffer (118 mM NaCl, 5 mM KCl, 1.2 mM $MgSO_4$, 2.5 mM $CaCl_2$, 1.53 mM KH_2PO_4, 212.7 mM glucose, and 1× protease inhibitor cocktail, pH 7.5). The homogenate was filtered through three 100-µm nylon filters (NY1H02500, Merck Millipore) and one 11 µm nylon filter (NY1102500, Merck Millipore). The filtrate was centrifuged at 1500 × *g* for 15 min at 4°C. The pellet obtained was resuspended in 1.2-ml synaptoneurosome buffer and used for APOE treatment.

Treatment with APOE and other drugs

Treatment of primary neurons

The primary neurons were treated with APOE from conditioned media or recombinant APOE protein (350-02, 350-04, Peprotech). For conditioned media treatment, the spent neuronal media was mixed with the APOE conditioned media in the ratio 1:1 such that the final APOE concentration used to treat the neurons was 10–20 nM. In case of recovery, the conditioned media mixture was removed and the spent neuronal media was added for recovery. For recombinant protein treatment, the neurons were treated with 15 nM of recombinant APOE3 or APOE4 protein in neurobasal media. In the experiments with no calcium in the external media, the neurons were treated with 15 nM recombinant APOE3 or APOE4 protein in artificial CSF (ACSF; 120 mM NaCl, 3 mM KCl, 1 mM $MgCl_2$, 3 mM $NaHCO_3$, 1.25 mM NaH_2PO_4, 15 mM HEPES, and 30 mM glucose, pH 7.4) with or without calcium (2 mM $CaCl_2$). For stimulation of NMDA receptors, 20 µM NMDA (0114, Tocris) was added during the last 5 min of the 20-min treatment. For the pretreatment with other drugs, nifedipine (50 µM; N7634, Sigma), dizocilpine (MK801; 25 µM; 0924, Tocris), or Receptor Associated Protein (RAP, 200nM; 553506 M, Sigma) were added for 10 min before the addition of conditioned media mixture. After the treatment, the cells were lysed in buffer containing 20 mM Tris-HCl, 100 mM KCl, 5 mM $MgCl_2$, 1% Nonidet P-40 (NP40), 1 mM dithiothreitol (dTT), 1× protease inhibitor cocktail, RNase inhibitor, 1× phosphatase inhibitor, and centrifuged at 20,000 × *g*, 4°C for 20 min. The supernatant was either denatured in sodium dodecyl sulphate (SDS)-dye for Western blotting or in TRIzol LS for RNA isolation.

Treatment of synaptoneurosomes

The resuspended synaptoneurosomes were treated with 15 nM recombinant APOE3 or APOE4 protein for 20 min at 37°C with mixing at 350 rpm. For stimulation of NMDARs in the synaptoneurosomes, NMDA (40 µM) was added during the last 5 min of the 20-min treatment. For blocking APOE receptors, RAP (200 nM) was added 10 min before the addition of APOE. After the treatment, the synaptoneurosomes were given a short spin, the pellet was resuspended in lysis buffer (20 mM Tris-HCl, 100 mM KCl, 5 mM $MgCl_2$, 1% NP40, 1 mM dTT, 1× protease inhibitor cocktail, RNase inhibitor, and 1× phosphatase inhibitor) and centrifuged at 20,000 × *g*, 4°C for 20 min. The supernatant was denatured in SDS-dye and subjected to Western blotting.

Mouse primary neuronal culture

Primary mouse neurons were generated from cortical and hippocampal tissue of wild-type embryos (E15–E17). Wild-type mouse embryos were obtained from pregnant B6.Cg-Tg (APPswe,PSEN1dE9)85Dbo/Mmjax mice (APP/PS1) mice, a widely used transgenic model of AD-like amyloidosis. The protocol used to generate primary neurons was previously described (Takahashi et al., 2004). In short, cortices and hippocampi were dissected, incubated in 0.25% trypsin for 15 min, and dissociated in DMEM containing 10% FBS (Invitrogen, 1008214) and 1% penicillin/streptomycin (ThermoFisher Scientific, SV3001). Dissociated primary cells were seeded on poly-D-lysine coated plates and maintained until 15 d *in vitro* (DIV) in Neurobasal medium with B27 supplement, 1.4 mM L-glutamine, and 1% penicillin/streptomycin.

Mouse primary astrocyte culture

Primary astrocyte cultures were obtained from ApoE3 knock-in (KI; B6.Cg-Apoe$^{em2(APOE*)Adiuj/J}$, The Jackson Laboratory, #029018), ApoE4 KI (B6(SJL)-Apoe$^{tm1.1(APOE*4)Adiuj/J}$, The Jackson Laboratory, #027894), and ApoE KO (B6.129P2-Apoe$^{<tm1Unc>/J}$, The Jackson Laboratory, #002052; Piedrahita et al., 1992) mouse brains. Cortical and hippocampal tissue was dissected from postnatal pups (P1–P3). After dissection, the brain tissue was incubated in 0.25% trypsin for 15 min. The tissue was dissociated into cells in DMEM containing 5% FBS (Invitrogen, 1008214) and 1% penicillin/streptomycin (ThermoFisher Scientific, SV3001) using soft plastic Pasteur pipettes. Primary cells were seeded at a concentration of 500,000 cells on poly-D-lysine coated T75 flasks; 3–5 h after seeding and culturing in DMEM medium containing 5% FBS and 1% P/S, the medium was replaced by AstroMACS medium (Miltenyi Biotec, 130-117-03) with 0.5 mM L-glutamine. AstroMACS medium of the primary astrocytes was replaced every 2–3 d. When at least 80% confluence of the primary astrocyte cultures was reached (around DIV12), the astrocytes were cultured in Neurobasal medium supplemented with B27, 1% penicillin/streptomycin, and 1.4 mM L-glutamine for 48 h for the collection of astrocyte conditioned medium. The conditioned astrocyte medium was used for the APOE treatment of the wild-type mouse primary neurons. The primary mouse neuron and astrocyte experiments were approved by the Ethical Committee for animal research at Lund University.

Fluorescent non-canonical amino acid tagging (FUNCAT)

For metabolic labeling, DIV15 neurons were incubated in Methionine-free DMEM for 45 min. Following this, the neurons were treated with L-azidohomoalanine (AHA; 1 µM; 1066100, Click Chemistry Tools) for 30 min in Met-free DMEM (21013024, ThermoFisher Scientific). They were then treated with 15 nM APOE3 or APOE4 recombinant protein in the same media (Met-free DMEM with AHA). For stimulation of NMDARs, NMDA (20 µM) was added during the last 5 min of the 20-min treatment. For FUNCAT assays with MK801 (25 µM) pretreatment, the drug was added during the last 20 min of AHA treatment. For FUNCAT assays with nifedipine (50 µM) pretreatment, the drug was added during the last 10 min of AHA treatment.

After the treatment, the coverslips were given one wash with 1× PBS and fixed with 4% paraformaldehyde (PFA). After 15 min of fixing, they were washed thrice with 1× PBS. The neurons were permeabilized for 10 min with 0.3% Triton X-100 solution prepared in TBS_{50} (50 mM Tris, 150 mM NaCl, pH 7.6). The permeabilized neurons were subjected to blocking for 1 h with a mixture of 2% bovine serum albumin (BSA) and 2% FBS prepared in TBS_{50}t (TBS50 with 0.1% Triton X-100). After blocking, the neurons were subjected to the FUNCAT reaction for 2 h where the newly-synthesized AHA incorporated proteins were tagged with an alkyne-fluorophore Alexa Fluor 555 through click reaction (C10269, CLICK-iT cell reaction buffer kit, Click Chemistry Tools). After three washes with TBS_{50}t, the neurons were stained with microtubule-associated protein 2 (MAP2) antibody (1:1000 dilution prepared in blocking buffer incubated overnight at 4°C) for detection of neuronal cells. This was followed by secondary antibody staining (1:500 dilution prepared in blocking buffer, incubated for 1 h at room temperature) to visualize MAP2.

For FUNCAT experiments with 1-min APOE treatment, 20-min APOE treatment, APOE treatment + NMDA stimulation, primary antibody MAP2 (M9942, Sigma) and corresponding secondary antibody Alexa Flour 488 were used. For FUNCAT experiments with NMDA stimulation time points, MK801+APOE treatment, nifedipine+APOE treatment, primary antibody MAP2 (ab32454, Abcam) and corresponding secondary antibody Alexa Flour 647 were used. Refer Table 1 for antibody details.

The coverslips were mounted with Mowiol 4–88 mounting media (81381, Sigma) and imaged on Olympus FV300 confocal laser scanning inverted microscope with 60× objective. The pinhole was kept at 1 airy unit and the optical zoom at 2× to satisfy Nyquist's sampling criteria in

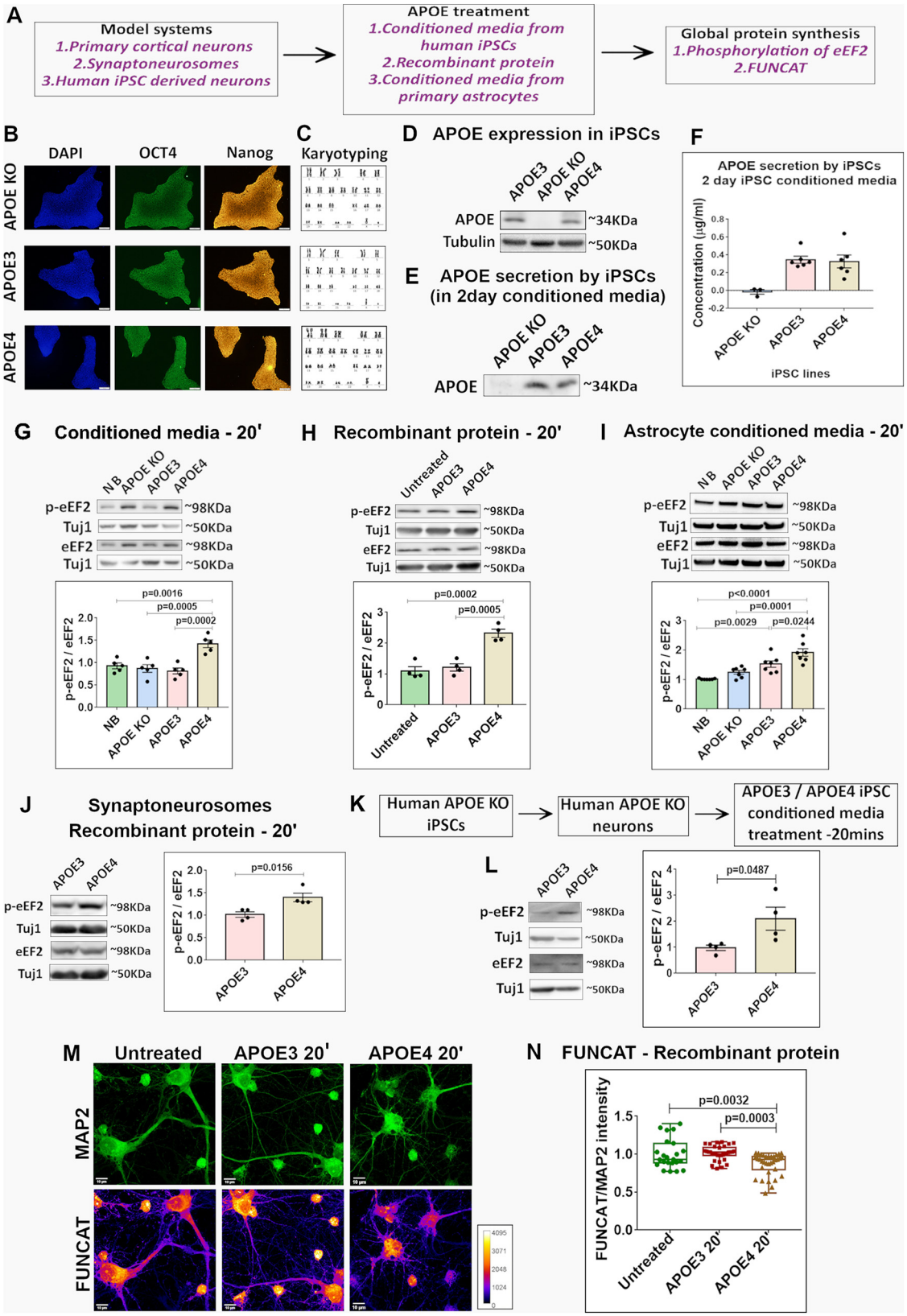

Figure 1. APOE4 treatment for 20 min decreases global protein synthesis in neurons and synaptoneurosomes. ***A***, Experimental workflow. Three different model systems primary cortical neurons, synaptoneurosomes or human iPSC derived neurons were treated with APOE from different sources: stem cell-secreted APOE, astrocyte-secreted APOE, and recombinant APOE protein. The APOE-treated neurons were probed for readouts of global protein synthesis. ***B***, APOE KO, APOE3, and APOE4 iPSCs were characterized for the expression of nuclear marker DAPI (left) and pluripotency markers OCT4 (middle) and NANOG (right). The representative images for the same are shown (scale bar: 10 μm). ***C***, The karyotyping profile of APOE KO, APOE3, and APOE4 iPSCs. ***D***, APOE KO, APOE3, and APOE4 iPSC cell lysates were probed for the expression of APOE. Representative immunoblots indicating the levels of APOE and loading control Tubulin are shown. ***E***, APOE KO, APOE3, and APOE4 iPSCs, on reaching 50% confluency, were maintained in neurobasal for 48 h. Representative immunoblots indicate the APOE secreted by the iPSCs in 2-d conditioned neurobasal media. ***F***, The amount of APOE secreted by the iPSCs in 2-d conditioned neurobasal media was estimated through ELISA. The graph indicates the average APOE concentration

XY direction. The objective was moved in *Z*-direction with a step size of 1 μM (approximately eight to nine Z-slices) to collect light from the planes above and below the focal plane. The image analysis was performed using FIJI software and the maximum intensity projection of the slices was used for quantification of the mean fluorescent intensities. The mean fluorescent intensity of the FUNCAT channel was normalized to the MAP2 channel for comparison between different APOE treatment conditions.

Immunostaining

The APOE iPSCs grown on four-well dishes were subjected to immunostaining of the pluripotency markers octamer-binding transcription factor 4 (OCT4) and NANOG. The iPSCs were fixed with 4% PFA which was followed by three washes with 1× PBS. This was followed by permeabilization with 0.3% Triton X-100 made in TBS_{50}. This was followed by 1-h blocking with 2% BSA and 2% FBS prepared in $TBS_{50}T$ (with 0.1% Triton X-100). They were incubated with the primary antibody (prepared in blocking buffer) overnight at 4°C. This was followed by three washes with $TSB_{50}T$ and 1-h incubation with the secondary antibody (prepared in blocking buffer) at room temperature. After three washes with $TBS_{50}T$, the iPSCs were subjected to postfixing with 4% PFA. This was followed by three washes with 1× PBS and then mounting with Mowiol 4–88 mounting media (81381, Sigma). The four well plates were imaged on Olympus IX73 inverted fluorescence microscope with 20× objective. Refer Table 1 for antibody details.

Western blotting

The APOE-treated neuron lysates or synaptoneurosome lysates were subjected to western blotting analysis. Briefly, the denatured lysates were run on 10% resolving and 5% stacking acrylamide gels and subjected to overnight transfer onto PVDF membrane. The blots were subjected to blocking for 1 h at room temperature using 5% BSA prepared in TBST (TBS with 0.1% Tween 20). This was followed by primary antibody (prepared in blocking buffer) incubation for 2–3 h at room temperature. Horseradish peroxidase (HRP) tagged secondary antibodies were used for primary antibody detection. The secondary antibodies (prepared in blocking buffer) were incubated with the blots for 1 h at room temperature. Three washes of 5–10 min each were given after primary and secondary antibody incubation using TBST solution. The blots were subjected to chemiluminescent-based detection of the HRP tagged proteins. For the analysis of eEF2 phosphorylation and extracellular-signal regulated kinase (ERK) phosphorylation, the samples were run in duplicates where one set was used to probe for the phospho-proteins (p-eEF2 and p-ERK), and the other set was used to probe for the total proteins (eEF2 and ERK). In each set, the loading control used was Tuj1. In every set, eEF2 and ERK were probed on the same blot. Hence, the Tuj1 used to normalize eEF2 and ERK was the same in a given set. Similarly, p-eEF2 and p-ERK were probed on the same blot for a given set. Hence, Tuj1 used to normalize them was also the same for the given set. For eIF2 phosphorylation analysis, the samples were run in duplicates (one set for phospho-protein, one set for total protein). Tuj1 was used as the normalizing control for each blot. For phosphatase and tensin homolog (PTEN) and PSD95 level analysis, PTEN and PSD95 were probed on the same blot and Tuj1 was used as the normalizing control for each set. For ribosomal protein lateral stalk subunit P0 (RPLP0) and RPS6 distribution analysis, the individual polysome fractions were run and used for percentage distribution quantification. All the western blot quantifications were performed using densitometric analysis on ImageJ software. Refer Table 2 for antibody details.

Polysome profiling

The DIV15 neurons (~1.5–2 million cells) were treated with APOE3 or APOE4 iPSC conditioned media for 20 min. For stimulation of NMDARs, NMDA (20 μM) was added during the last 5 min of the 20-min treatment. After the treatment, the cells were lysed in buffer containing 20 mM Tris-HCl, 100 mM KCl, 5 mM $MgCl_2$, 1% NP40, 1 mM dTT, 1× Protease Inhibitor Cocktail, RNase inhibitor, 0.1 mg/ml cycloheximide (CHX; C7698, Sigma), 1× Phosphatase Inhibitor and centrifuged at 20,000 × *g*, 4°C for 20 min. The supernatant was loaded on 15%−45% linear sucrose gradient prepared in buffer containing 20 mM Tris-HCl, 100 mM KCl, 5 mM $MgCl_2$, 0.1 mg/ml Cycloheximide. The gradients loaded with the lysates were subjected to ultracentrifugation at 39,000 rpm, 4°C for 1.5 h. 1 ml fractions were collected from the gradient after the spin (11 fractions in total), as the fractions were collected, they were passed through a UV spectrophotometer to obtain the absorbance profile at 254 nm. The individual fractions were subjected to Western blotting to probe for ribosomal protein RPLP0 and RNA isolation/quantitative PCR to probe for candidate mRNAs.

To identify actively translating polysomes, the cells were treated with 1 mM puromycin (P8833, Sigma) and lysed in the buffer containing puromycin instead of CHX. The puromycin-sensitive fractions 7–11 were considered as the actively translating fractions whereas the puromycin-insensitive fractions 1–6 were considered as the non-translating pool. The ratio was considered as shown: ratio of (translating pool/non-translating pool) = ratio of (sum of percentage of mRNA or protein in fractions 7–11/sum of percentage of mRNA or protein in fractions 1–6).

To further dissect the distribution of mRNAs/proteins in the non-translating pool, fractions 1–6 were further divided into fractions 1–3 (inhibitory complex) and fractions 4–6 (ribosomal subunits and monosomes; note: in this case, the percentage was calculated with respect to distribution in fractions 1–6). The enrichment of the mRNAs/proteins in the inhibitory complex was calculated as: sum of percentage of mRNAs or proteins in fractions 1–3/sum of percentage of mRNAs or proteins in fractions 4–6. Refer Table 3 for primer details.

Calcium imaging

Calcium imaging was done on DIV15 neurons plated on Nunc glass-bottomed imaging dishes. The imaging and washes were performed with ACSF media (120 mM NaCl, 3 mM KCl, 1 mM $MgCl_2$, 3 mM $NaHCO_3$, 1.25 mM NaH_2PO_4, 15 mM HEPES, 2 mM $CaCl_2$, and 30 mM glucose, pH 7.4). The cells were washed once with ACSF and incubated at 37°C with

←

(μg/ml) in 2-d iPSC conditioned media. Data is represented as Mean ± SEM. ***G***, Rat primary cortical neurons (DIV15) were treated with APOE (10–15 nM) from iPSC conditioned media for 20 min and probed for phosphorylation of eEF2. Top, Representative immunoblots indicating levels of phospho-eEF2, eEF2, and Tuj1. Bottom, Graph indicating ratio of phospho-eEF2 to eEF2 normalized to Tuj1. Data are represented as mean ± SEM, $N = 5$, one-way ANOVA ($p = 0.0001$) followed by Tukey's multiple comparison test. ***H***, Rat primary cortical neurons (DIV15) were treated with recombinant APOE protein (15 nM) for 20 min and probed for phosphorylation of eEF2. Top, Representative immunoblots indicating levels of phospho-eEF2, eEF2, and Tuj1. Bottom, Graph indicating ratio of phospho-eEF2 to eEF2 normalized to Tuj1. Data are represented as mean ± SEM, $N = 4$, one-way ANOVA ($p = 0.0002$) followed by Tukey's multiple comparison test. ***I***, Mouse primary cortical neurons (DIV15) were treated with APOE from mouse primary astrocyte conditioned media for 20 min and probed for phosphorylation of eEF2. Top, Representative immunoblots indicating levels of phospho-eEF2, eEF2, and Tuj1. Bottom, Graph indicating ratio of phospho-eEF2 to eEF2 normalized to Tuj1. Data are represented as mean ± SEM, $N = 7$, one-way ANOVA ($p < 0.0001$) followed by Tukey's multiple comparison test. ***J***, Synaptoneurosomes prepared from P30 rat cortices were treated with recombinant APOE protein (15 nM) for 20 min and probed for phosphorylation of eEF2. Left, Representative immunoblots indicating levels of phospho-eEF2, eEF2, and Tuj1. Right, Graph indicating ratio of phospho-eEF2 to eEF2 normalized to Tuj1. Data are represented as mean ± SEM, $N = 4$, unpaired Student's *t* test. ***K***, Experimental workflow. Human APOE KO neurons derived from human APOE KO iPSCs were subjected to APOE3 or APOE4 iPSC conditioned media treatment for 20 min and probed for phosphorylation of eEF2. ***L***, Human APOE KO neurons (four weeks into neuronal maturation) were treated with APOE3/APOE4 (10–15 nM) iPSC conditioned media for 20 min and probed for the phosphorylation of eEF2. Left, Representative immunoblots indicating levels of phospho-eEF2, eEF2, and Tuj1. Right, Graph indicating ratio of phospho-eEF2 to eEF2 normalized to Tuj1. Data are represented as mean ± SEM, $N = 4$, unpaired Student's *t* test. ***M***, Rat primary cortical neurons (DIV15) were treated with recombinant APOE protein (15 nM) for 20 min and subjected to FUNCAT along with immunostaining for MAP2. The representative images for MAP2 and FUNCAT fluorescent signal under different APOE treatment conditions are shown (scale bar: 10 μm). ***N***, The graph represents the quantification of the FUNCAT fluorescent intensity normalized to MAP2 fluorescent intensity under different APOE treatment conditions. Each data point represents an individual neuron. $N = 20–40$ neurons from 4 independent experiments, one-way ANOVA ($p = 0.0001$) followed by Tukey's multiple comparison test.

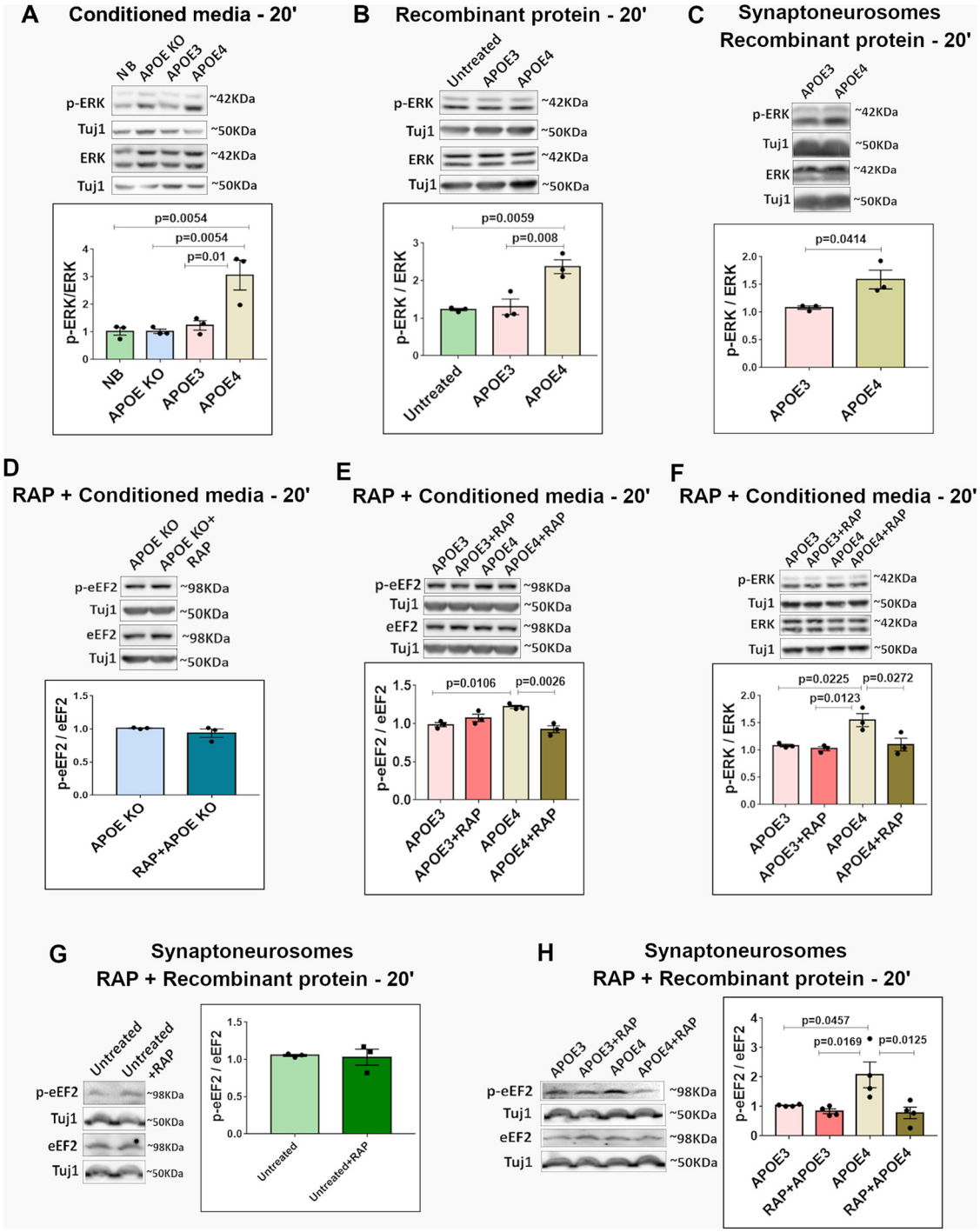

Figure 2. APOE4-induced increase in eEF2 phosphorylation is mediated through APOE receptors. ***A***, Rat primary cortical neurons (DIV15) were treated with APOE (10–15 nM) from iPSC conditioned media for 20 min and probed for the phosphorylation of ERK. Top, Representative immunoblots indicating levels of phospho-ERK, ERK, and Tuj1. Bottom, Graph indicating ratio of phospho-ERK to ERK normalized to Tuj1. Data are represented as mean ± SEM, $N = 3$, one-way ANOVA ($p = 0.0031$) followed by Tukey's multiple comparison test. ***B***, Rat primary cortical neurons (DIV15) were treated with recombinant APOE protein (15 nM) for 20 min and probed for the phosphorylation of ERK. Top, Representative immunoblots indicating levels of phospho-ERK, ERK, and Tuj1. Bottom, Graph indicating ratio of phospho-ERK to ERK normalized to Tuj1. Data are represented as mean ± SEM, $N = 3$, one-way ANOVA ($p = 0.0041$) followed by Tukey's multiple comparison test. ***C***, Synaptoneurosomes prepared from P30 rat cortices were treated with recombinant APOE protein (15 nM) for 20 min and probed for the phosphorylation of ERK. Top, Representative immunoblots indicating levels of phospho-ERK, ERK, and Tuj1. Bottom, Graph indicating ratio of phospho-ERK to ERK normalized to Tuj1. Data are represented as mean ± SEM, $N = 3$, unpaired Student's t test. ***D***, Rat primary cortical neurons (DIV15) were treated with APOE receptor antagonist RAP (200 nM) along with APOE KO conditioned media for 20 min and probed for the phosphorylation of eEF2. Top, Representative immunoblots indicating levels of phospho-eEF2, eEF2, and Tuj1. Bottom, Graph indicating ratio of phospho-eEF2 to eEF2 normalized to Tuj1. Data are represented as mean ± SEM, $N = 3$, unpaired Student's t test. ***E***, Rat primary cortical neurons (DIV15) were treated with APOE receptor antagonist RAP (200 nM) along with APOE3/APOE4 (10–15 nM) from iPSC conditioned media for 20 min and probed for phosphorylation of eEF2. Top, Representative immunoblots indicating levels of phospho-eEF2, eEF2, and Tuj1. Bottom, Graph indicating ratio of phospho-eEF2 to eEF2 normalized to Tuj1. Data are represented as mean ± SEM, $N = 5$, one-way ANOVA ($p = 0.003$) followed by Tukey's multiple comparison test. ***F***, Rat primary cortical neurons (DIV15) were treated with APOE receptor antagonist RAP (200 nM) along with APOE3/APOE4 (10–15 nM) from iPSC conditioned media for 20 min and probed for the phosphorylation of ERK. Left, Representative immunoblots indicating levels of phospho-ERK, ERK, and Tuj1. Right, Graph indicating ratio of phospho-ERK to ERK normalized to Tuj1. Data are represented as mean ± SEM, $N = 3$, one-way ANOVA ($p = 0.0097$) followed by Tukey's multiple comparison test. ***G***, Synaptoneurosomes prepared from P30 rat cortices were

1 ml of freshly prepared Fluo4-AM dye solution (1 μM Fluo4-AM and 0.002% pluronic acid in ACSF; F14217, ThermoFisher Scientific) for 20 min. They were given two washes and incubated in ACSF at 37°C for 10–20 min before imaging. The drugs nifedipine (50 μM) and MK801 (25 μM) were added during this incubation step. The neurons were imaged using Olympus FV300 confocal laser scanning inverted microscope with 20× objective, illuminated with 488 nm lasers. The neurons were imaged for a total time of 7 min at a rate of 3 s per frame (140 frames in total). They were imaged in basal condition for 1 min (20 frames). Following that, they were imaged for 5 min (100 frames) with APOE recombinant protein (20 nM) addition. Finally, they were imaged for 1 min (20 frames) with the addition of Ionomycin solution (10 μM ionomycin with 10 mM $CaCl_2$; 407950, Sigma). The images obtained were analyzed using the Time-Series Analyzer plug-in on FIJI software. The average intensities were obtained for the selected regions of interest (ROIs; ROIs were drawn manually and the Ionomycin responsive cells were included). The change in fluorescent intensity at each frame was normalized to the initial fluorescent intensity of the first frame (F0) for each ROI. The normalized change in fluorescent intensity (ΔF/F0) was plotted along the time axis and used for statistical analysis as well.

Differentiation of iPSCs to neurons

The protocol for neural differentiation was adapted from Shi et al. (2012) and Zhang et al. (2017) with some modifications. In brief, iPSCs were expanded in mTeSR until 70–80% confluency was reached. The neural basic media (NBM) for differentiation contained 50% DMEM F-12 (21331-020, ThermoFisher Scientific), 50% Neurobasal, 0.1% PenStrep, Glutamax, N2 (17502-048, ThermoFisher Scientific), and B27 without Vitamin A (12587-010, ThermoFisher Scientific). The iPSCs were subjected to monolayer Dual SMAD inhibition by changing the media to neural induction media (NIM) which is composed of NBM supplemented with small molecules SB431542 (10 μM, an inhibitor of TGFβ pathway; 72232, Stem Cell Technologies) and LDN193189 (0.1 μM, an inhibitor of BMP pathway; 72142, Stem Cell Technologies). The cells were subjected to neural induction for 12–15 d by changing the NIM every day. After the induction, the monolayer was dissociated using Accutase (A6964, Sigma) and the cells were plated in NIM containing 10 μM ROCK inhibitor (Y0503, Sigma) overnight on precoated poly-L-ornithine/laminin dishes. Poly-L-ornithine (1:10 dilution; P4957, Sigma) followed by laminin (5 μg/ml; L2020, Sigma) coating was used for maintenance of neural progenitors and their terminal differentiation. Expansion of the neural progenitor cells was conducted in neural expansion media (NEM) which is composed of NBM supplemented with fibroblast growth factor (FGF; 10 ng/ml; 100-18C, Peprotech) and epidermal growth factor (EGF; 10 ng/ml; AF-100-15, Pepotech). Neuronal maturation and terminal differentiation were achieved by plating the neural stem cells at a density of 25,000–35,000 cells/cm^2 in the neural maturation media (NMM) composed of NBM supplemented with brain-derived neurotrophic factor (BDNF; 20 ng/ml; 450-02, Peprotech), glial-derived neurotrophic factor (GDNF; 10 ng/ml; 450-10, Peprotech), L-ascorbic acid (200 μM; A4403, Sigma), and db-Camp (50 μM; D0627, Sigma). The neurons were subjected to maturation for a period of four to five weeks by supplementing them with NMM every 4–5 d.

Statistical analyses

All statistical analyses were performed using GraphPad Prism software. The normality of the data was checked using the Kolmogorov–Smirnov test. For experiments with less than five data points, parametric statistical tests were applied. Data were represented as mean ± SEM in all biochemical experiment graphs. FUNCAT and calcium imaging data were represented as boxes and whiskers with all the individual data points. Statistical significance was calculated using unpaired Student's *t* test (two-tailed with equal variance) in cases where two groups were being compared. One-way ANOVA was used for multiple group comparisons, followed by Tukey's multiple comparison test or Dunnett's multiple comparison test; $p < 0.05$ was considered to be statistically significant.

Table 1. Antibodies used for immunostaining

Protein	Dilution	Catalog number, company
MAP2	1:1000	M9942, Sigma
MAP2	1:1000	ab32454, Abcam
OCT4	1:500	sc-5279, Santa Cruz
Nanog	1:500	500-P236, Peprotech
Alexa Fluor 488	1:500	A-11059, ThermoFisher Scientific
Alexa Fluor 555	1:500	A-21428, ThermoFisher Scientific
Alexa Flour 647	1:500	A27040, ThermoFisher Scientific

Table 2. Antibodies used for Western blotting

Protein	Dilution	Catalog number, company
eEF2	1:1000	2332S, Cell Signaling Technologies
p-eEF2	1:2000	2331S, Cell Signaling Technologies
ERK	1:1000	9102, Cell Signaling Technologies
p-ERK	1:1000	9101, Cell Signaling Technologies
APOE	1:1000	NB110-60531, Novus Biologicals
Tuj1	1:4000	T8578, Sigma
RPLP0	1:4000	ab101279, Abcam
RPS6	1:3000	2217, Cell Signaling Technologies
PTEN	1:1000	9552S, Cell Signaling Technologies
PSD95	1:1000	P246, Sigma
α-tubulin	1:5000	T9026, Sigma
eIF2	1:1000	9722S, Cell Signaling Technologies
p-eIF2	1:1000	9721S, Cell Signaling Technologies
Secondary rabbit HRP	1:5000	A0545, Sigma
Secondary mouse HRP	1:5000	31430, ThermoFisher Scientific

Table 3. Primers used for RT-PCR

mRNA	Forward primer (5′→3′)	Reverse primer (5′→3′)
PTEN	AGGACCAGAGATAAAAAGGGAGT	CCTTTAGCTGGCAGACCACA
PSD95	ATGGCAGGTTGCAGATTGGA	GGTTGTGATGTCTGGGGGAG
β-Actin	GGCTCCTAGCACCATGAAGAT	AAACGCAGCTCAGTAACAGTC
α-Tubulin	TATGCCAAGCGTGCCTTTGT	TGAAAGCAGCACCTTGTGAC

Results

APOE4 causes a reduction of protein synthesis in neurons

Activity-mediated protein synthesis is a dynamic process which impacts both short-term and long-term aspects of synaptic function and plasticity (Sutton and Schuman, 2006). APOE4 was previously shown to disrupt many synaptic functions (Wang et al., 2005; Dumanis et al., 2009; Chen et al., 2010; Liu et al., 2015), but its impact on protein synthesis in neurons has not been studied extensively. To study the effect of APOE4 on global and activity-mediated protein synthesis in neurons, we used cultured primary cortical neurons (DIV15) from SD rats as our primary model system (Fig. 1*A*). We have further validated our findings in synaptoneurosomes and human stem cell derived neuron model systems (Fig. 1*A*). We used conditioned or secreted media from human iPSCs (hiPSCs) as one of the main sources of

←

treated with APOE receptor antagonist RAP (200 nM) for 20 min and probed for the phosphorylation of eEF2. Left, Representative immunoblots indicating levels of phospho-eEF2, eEF2, and Tuj1. Right, Graph indicating ratio of phospho-eEF2 to eEF2 normalized to Tuj1. Data are represented as mean ± SEM, $N = 3$, unpaired Student's *t* test. ***H***, Synaptoneurosomes prepared from P30 rat cortices were treated with APOE receptor antagonist RAP (200 nM) along with recombinant APOE protein (15 nM) for 20 min and probed for the phosphorylation of eEF2. Left, Representative immunoblots indicating levels of phospho-eEF2, eEF2, and Tuj1. Right, Graph indicating ratio of phospho-eEF2 to eEF2 normalized to Tuj1. Data are represented as mean ± SEM, $N = 4$, one-way ANOVA ($p = 0.0088$) followed by Tukey's multiple comparison test.

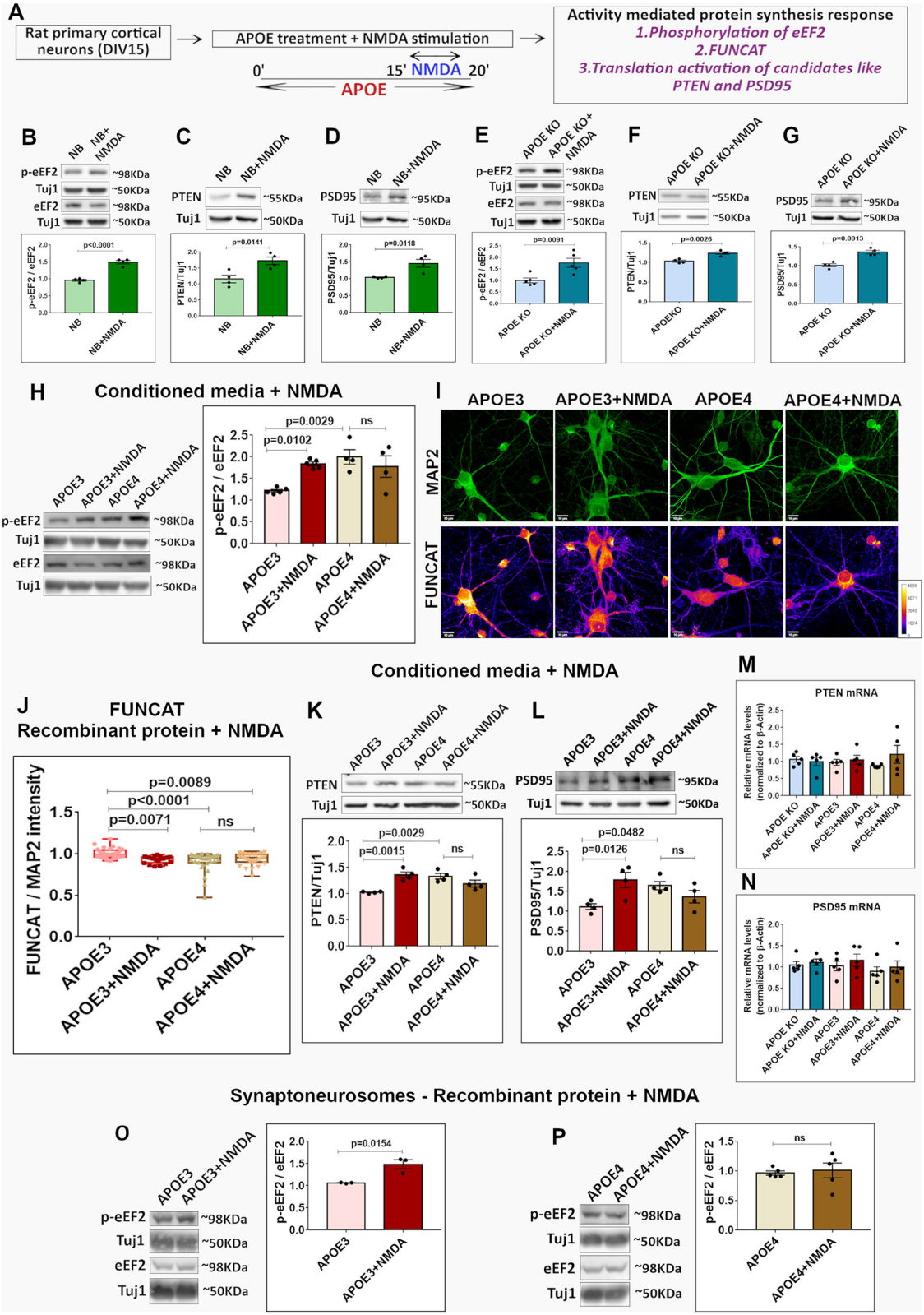

Figure 3. The NMDAR-mediated translation response is lost in APOE4-treated neurons. ***A***, Experimental workflow. Rat primary cortical neurons (DIV15) were treated with APOE from iPSC conditioned media/recombinant protein for 20 min. During the last 5 min of the APOE treatment, the neurons were subjected to stimulation of NMDARs (20 μM NMDA, 5 min). The NMDAR-mediated translation response in APOE-treated neurons was probed by using the following readouts: phosphorylation of eEF2, FUNCAT, and increased levels of PTEN and PSD95 proteins. ***B***, Rat primary cortical neurons (DIV15) were treated with neurobasal media for 20 min along with NMDAR stimulation for 5 min (20 μM NMDA) and probed for the phosphorylation of eEF2. Top, Representative immunoblots indicating levels of phospho-eEF2, eEF2, and Tuj1. Bottom, Graph indicating ratio of phospho-eEF2 to eEF2 normalized to Tuj1. Data are represented as mean ± SEM, $N = 4$, unpaired Student's t test. ***C***, Rat primary cortical neurons (DIV15) were treated with neurobasal media for 20 min along with NMDAR stimulation for 5 min (20 μM NMDA) and probed for PTEN protein levels. Top, Representative immunoblots indicating levels of PTEN and Tuj1. Bottom, Graph indicating PTEN levels normalized to Tuj1. Data are represented as mean ± SEM, $N = 4$, unpaired Student's t test. ***D***, Rat primary cortical neurons (DIV15) were treated with neurobasal media for 20 min along with NMDAR stimulation for 5 min (20 μM NMDA) and

APOE in our study (Fig. 1*A*). iPSC lines of different APOE genotypes (APOE3/3, APOE4/4, and APOE KO) were generated by CRISPR-Cas9-based editing of the original APOE3/4 iPSC line (Schmid et al., 2019). These iPSCs were characterized for the expression of the pluripotency markers (OCT4 and Nanog) and normal karyotype profile (Fig. 1*B*, *C*). When the iPSCs reached 50% confluency, they were switched from stem cell medium to neurobasal medium. After 48 h, the conditioned neurobasal media containing APOE protein was collected from the stem cells. The iPSCs express a significant amount of APOE protein (Fig. 1*D*) and the APOE secreted by the iPSCs into the neurobasal media was stable for at least 48 h (Fig. 1*E*). The average concentration of APOE secreted in the conditioned neurobasal media was 0.2–0.3 μg/ml as measured by ELISA (Fig. 1*F*). We also used two other sources of APOE (astrocyte conditioned media and recombinant protein) to strengthen our results (Fig. 1*A*). The readouts used for global protein synthesis measurements were phosphorylation status of eukaryotic translation elongation factor eEF2 (increase in eEF2 phosphorylation implies translation inhibition) and FUNCAT (decrease in FUNCAT signal implies translation inhibition; Fig. 1*A*; Tom Dieck et al., 2012; Heise et al., 2014; Ghosh Dastidar et al., 2020).

In the first experiment, we treated the rat primary cortical neurons with neurobasal media or conditioned neurobasal media from APOE KO, APOE3, or APOE4 iPSCs (final concentration of APOE was 10–15 nM) for 20 min (Fig. 1*G*). APOE4 conditioned media treatment for 20 min caused a significant 1.5-fold increase in eEF2 phosphorylation compared with APOE3, APOE KO, and untreated conditions (Fig. 1*G*). Treatment with APOE3 (the most common APOE variant in the human population) did not cause any change in eEF2 phosphorylation compared with APOE KO treatment or untreated conditions (Fig. 1*G*). This indicated that there could be a significant reduction of protein synthesis in the neurons exposed to APOE4 for 20 min. The same response was observed when the neurons were treated with recombinant APOE protein instead of conditioned media at a similar concentration (15 nM). With recombinant APOE4 treatment for 20 min, a significant increase in eEF2 phosphorylation was observed compared with both untreated and APOE3-treated neurons (Fig. 1*H*). Since APOE is primarily secreted by astrocytes in the brain, we wanted to investigate whether APOE4 secreted from *in vitro* cultured astrocytes has the same effect on neuronal translation as APOE4 secreted by iPSCs. To study this, we cultured primary astrocytes from APOE KO mice or humanized APOE 3/3 or APOE 4/4 KI mice and collected the APOE astrocyte conditioned media. The primary cultured neurons (DIV15) from C57Bl/6 mice were exposed to the mouse APOE astrocyte conditioned media for 20 min and the translation status was measured by the phosphorylation of eEF2. We observed a significant increase in the phosphorylation of eEF2 in mouse neurons exposed to APOE4 astrocyte conditioned media as compared with APOE3 or APOE KO astrocyte conditioned media and neurobasal conditions (Fig. 1*I*), further validating the effect of APOE4 on translation.

To test whether the APOE4-induced translation inhibition occurs in the synaptic compartments, we prepared synaptoneurosomes from P30 rat cortices and treated them with 15 nM recombinant APOE protein for 20 min. We observed a significant increase in eEF2 phosphorylation in the synaptoneurosomes exposed to APOE4 recombinant protein as compared with APOE3 (Fig. 1*J*). Additionally, we verified our findings in the human stem cell derived neuron system. Human APOE KO neurons derived from APOE KO iPSCs were treated with APOE3 or APOE4 iPSC conditioned media for 20 min and probed for eEF2 phosphorylation (Fig. 1*K*). APOE4 conditioned media treatment for 20 min caused a significant increase in eEF2 phosphorylation compared with APOE3 treatment in the human neuron system

←

probed for PSD95 protein levels. Top, Representative immunoblots indicating levels of PSD95 and Tuj1. Bottom, Graph indicating PSD95 levels normalized to Tuj1. Data are represented as mean ± SEM, $N = 4$, unpaired Student's t test. ***E***, Rat primary cortical neurons (DIV15) were treated with APOE KO conditioned media for 20 min along with NMDAR stimulation for 5 min (20 μM NMDA) and probed for the phosphorylation of eEF2. Top, Representative immunoblots indicating levels of phospho-eEF2, eEF2, and Tuj1. Bottom, Graph indicating ratio of phospho-eEF2 to eEF2 normalized to Tuj1. Data are represented as mean ± SEM, $N = 5$, unpaired Student's t test. ***F***, Rat primary cortical neurons (DIV15) were treated with APOE KO conditioned media for 20 min along with NMDAR stimulation for 5 min (20 μM NMDA) and probed for PTEN protein levels. Top, Representative immunoblots indicating levels of PTEN and Tuj1. Bottom, Graph indicating PTEN levels normalized to Tuj1. Data are represented as mean ± SEM, $N = 4$, unpaired Student's t test. ***G***, Rat primary cortical neurons (DIV15) were treated with APOE KO conditioned media for 20 min along with NMDAR stimulation for 5 min (20 μM NMDA) and probed for PSD95 protein levels. Top, Representative immunoblots indicating levels of PSD95 and Tuj1. Bottom, Graph indicating PSD95 levels normalized to Tuj1. Data are represented as mean ± SEM, $N = 4$, unpaired Student's t test. ***H***, Rat primary cortical neurons (DIV15) were treated with APOE3/APOE4 (10–15 nM) conditioned media for 20 min along with NMDAR stimulation for 5 min (20 μM NMDA) and probed for the phosphorylation of eEF2. Left, Representative immunoblots indicating levels of phospho-eEF2, eEF2, and Tuj1. Right, Graph indicating ratio of phospho-eEF2 to eEF2 normalized to Tuj1. Data are represented as mean ± SEM, $N = 4$–5, one-way ANOVA ($p = 0.0047$) followed by Dunnett's multiple comparison test, ns in the figure implies non-significant. ***I***, Rat primary cortical neurons (DIV15) were treated with recombinant APOE3 or APOE4 protein (15 nM) for 20 min along with NMDAR stimulation for 5 min (20 μM NMDA). They were subjected to FUNCAT along with immunostaining for MAP2. The representative images for MAP2 and FUNCAT fluorescent signal under different treatment conditions are shown (scale bar: 10 μm). ***J***, The graph represents the quantification of the FUNCAT fluorescent intensity normalized to MAP2 fluorescent intensity under different treatment conditions. Each data point represents an individual neuron. $N = 20$–40 neurons from 2 independent experiments, one-way ANOVA ($p < 0.0001$) followed by Tukey's multiple comparison test, ns in the figure implies non-significant. ***K***, Rat primary cortical neurons (DIV15) were treated with APOE3/APOE4 (10–15 nM) conditioned media for 20 min along with NMDAR stimulation for 5 min (20 μM NMDA) and probed for PTEN protein levels. Top, Representative immunoblots indicating levels of PTEN and Tuj1. Bottom, Graph indicating PTEN levels normalized to Tuj1. Data are represented as mean ± SEM, $N = 4$, one-way ANOVA ($p = 0.002$) followed by Dunnett's multiple comparison test, ns in the figure implies non-significant. ***L***, Rat primary cortical neurons (DIV15) were treated with APOE3/APOE4 (10–15 nM) conditioned media for 20 min along with NMDAR stimulation for 5 min (20 μM NMDA) and probed for PSD95 protein levels. Top, Representative immunoblots indicating levels of PSD95 and Tuj1. Bottom, Graph indicating PSD95 levels normalized to Tuj1. Data are represented as mean ± SEM, $N = 4$, one-way ANOVA ($p = 0.0216$) followed by Dunnett's multiple comparison test, ns in the figure implies non-significant. ***M***, Rat primary cortical neurons (DIV15) were treated with APOE KO/APOE3/APOE4 (10–15 nM) conditioned media for 20 min along with NMDAR stimulation for 5 min (20 μM NMDA) and subjected to RT-PCR to measure the levels of PTEN mRNA. The graph indicates the copy number of PTEN mRNA normalized to copy number of β-actin mRNA under different treatment conditions. Data are represented as mean ± SEM, $N = 5$, one-way ANOVA (ns - non-significant). ***N***, Rat primary cortical neurons (DIV15) were treated with APOE KO/APOE3/APOE4 (10–15 nM) conditioned media for 20 min along with NMDAR stimulation for 5 min (20 μM NMDA) and subjected to RT-PCR to measure the levels of PSD95 mRNA. The graph indicates the copy number of PSD95 mRNA normalized to copy number of β-actin mRNA under different treatment conditions. Data are represented as mean ± SEM, $N = 5$, one-way ANOVA (ns - non-significant). ***O***, Synaptoneurosomes prepared from P30 rat cortices were treated with recombinant APOE3 protein (15 nM) for 20 min along with NMDAR stimulation for 5 min (40 μM NMDA) and probed for the phosphorylation of eEF2. Left, Representative immunoblots indicating levels of phospho-eEF2, eEF2, and Tuj1. Right, Graph indicating ratio of phospho-eEF2 to eEF2 normalized to Tuj1. Data are represented as mean ± SEM, $N = 3$, unpaired Student's t test. ***P***, Synaptoneurosomes prepared from P30 rat cortices were treated with recombinant APOE4 protein (15 nM) for 20 min along with NMDAR stimulation for 5 min (40 μM NMDA) and probed for the phosphorylation of eEF2. Left, Representative immunoblots indicating levels of phospho-eEF2, eEF2, and Tuj1. Right, Graph indicating ratio of phospho-eEF2 to eEF2 normalized to Tuj1. Data are represented as mean ± SEM, $N = 5$, unpaired Student's t test, ns in the figure implies non-significant.

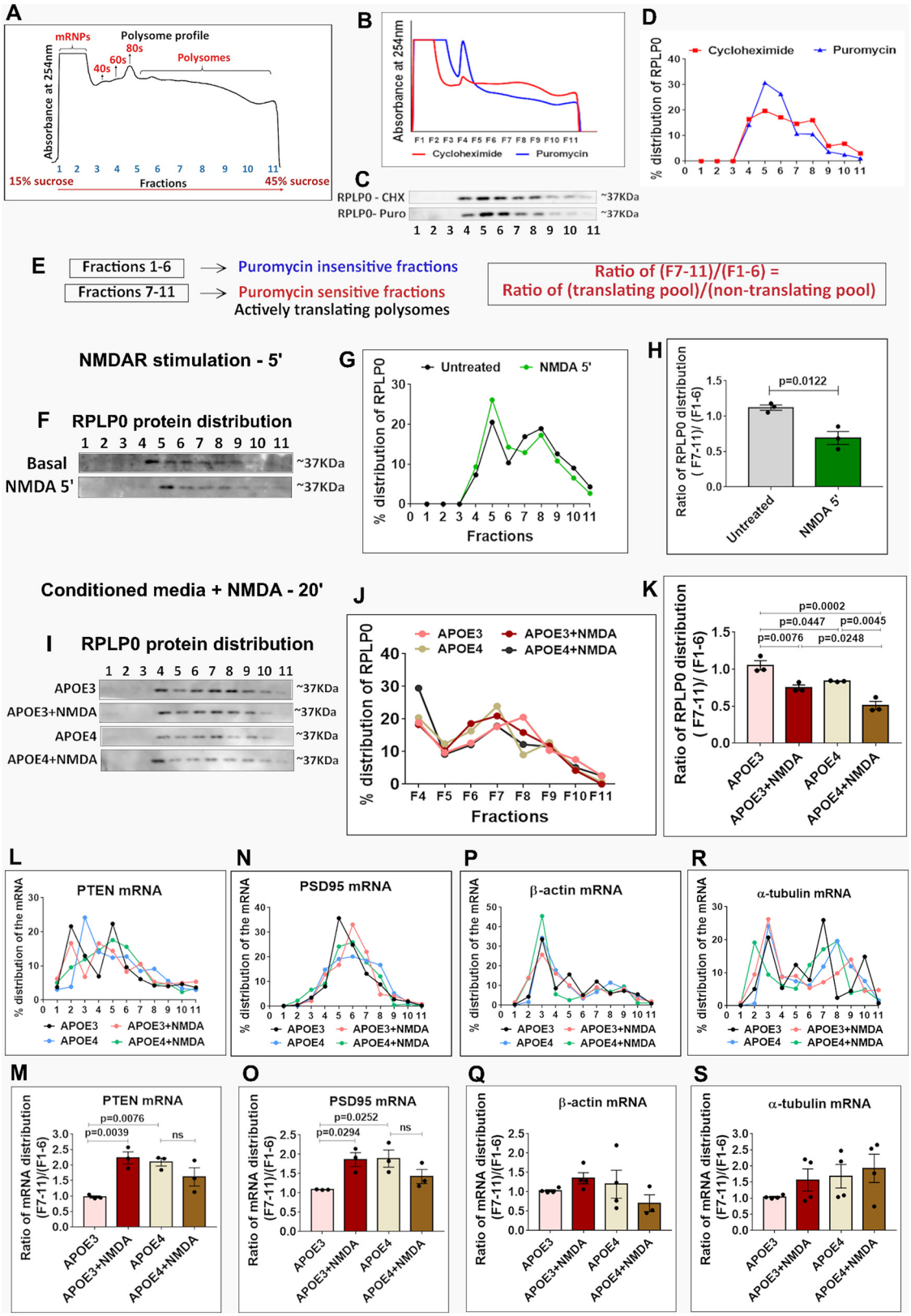

Figure 4. 20-min treatment of neurons with APOE4 mimics the 5-min NMDAR response of global protein synthesis inhibition and translation activation of specific candidate mRNAs. ***A***, Representative polysome profile or absorbance profile at 254 nm indicating the mRNPs, ribosomal subunits (40S, 60S), monosomes (80S), and polysomes distributed on 15–45% linear sucrose gradient. ***B***, Rat primary cortical neurons (DIV15) were subjected to polysome profiling after treatment with Cycloheximide (CHX) and Puromycin (Puro). The graph represents the polysome profile or absorbance profile at 254 nm under CHX and Puro conditions. ***C***, The immunoblots show the distribution of ribosomal protein RPLP0 in the individual fractions on CHX and Puro treatment conditions. ***D***, The graph represents the percentage distribution of RPLP0 in each fraction under CHX and Puro treatment conditions. ***E***, Schematic showing the division of polysome profiling fractions into two pools based on sensitivity to puromycin treatment. Fractions 7–11 were the puromycin sensitive or actively translating pool and fractions 1–6 were the puromycin insensitive pool or non-translating pool. The ratio of the percentage of protein or mRNA in fractions 7–11/fractions 1–6 indicates their distribution in the translating pool/non-translating pool. ***F***, Rat

as well (Fig. 1*L*), further supporting the finding of global translation inhibition by APOE4.

Since the phosphorylation of eEF2 indicates the translation status at a given time point, we used the FUNCAT assay, a more direct readout for translation, to measure the cumulative effect of APOE4 exposure on protein synthesis for 20 min in neurons. Neurons treated with recombinant APOE4 protein for 20 min showed a significant reduction in the FUNCAT signal compared with APOE3-treated or untreated neurons (Fig. 1*M*,*N*), thus corroborating the global decrease of protein synthesis in neurons exposed to APOE4. In summary, we have shown that APOE4 exposure for 20 min caused a significant reduction of protein synthesis in primary neurons, human stem cell derived neurons and synaptoneurosomal preparations. We have demonstrated this by using APOE from multiple sources including iPSC conditioned media, astrocyte conditioned media, and recombinant protein.

Reduction of protein synthesis on APOE4 treatment is mediated through APOE receptors

We validated our APOE treatment paradigm by measuring the phosphorylation of ERK, a feature previously reported on APOE exposure (Huang et al., 2017, 2019). We observed an increase in ERK phosphorylation in the neurons exposed to APOE4 conditioned media or APOE4 recombinant protein for 20 min (Fig. 2*A*,*B*). However, 20-min treatment with APOE3/APOE KO conditioned media or APOE3 recombinant protein did not cause a change in ERK phosphorylation as compared with control conditions (Fig. 2*A*,*B*). We also observed the increase in ERK phosphorylation in synaptoneurosomes treated with recombinant APOE4 protein for 20 min, as compared with APOE3 treatment (Fig. 2*C*).

To confirm that the effect of APOE on translation was mediated through the binding of APOE to its cognate receptor, we inhibited the APOE receptor using its antagonist receptor-associated protein (RAP). In the presence of RAP, APOE4-induced increase in the phosphorylation of eEF2 was blocked (Fig. 2*E*). However, RAP did not have any effect on eEF2 phosphorylation when treated with APOE3 conditioned media (Fig. 2*E*) or APOE KO conditioned media (Fig. 2*D*). Similarly, RAP was able to completely prevent the APOE4-mediated increase in the phosphorylation of ERK (Fig. 2*F*), whereas RAP had no effect on ERK phosphorylation on APOE3 treatment (Fig. 2*F*).

Additionally, RAP prevented the APOE4-mediated increase in eEF2 phosphorylation in synaptoneurosomes as well (Fig. 2*H*), further validating that the APOE4-mediated translation inhibition was synaptic and mediated through APOE receptors. RAP treatment of synaptoneurosomes in the absence of APOE had no effect on eEF2 phosphorylation (Fig. 2*G*). Thus, we validated that the translation inhibition caused by APOE4 is specifically because of the binding of APOE to its cognate receptors in the neurons.

NMDAR-mediated translation response is completely lost on APOE4 exposure

APOE4 was previously reported to interfere with NMDAR signaling (Qiu et al., 2003; Hoe et al., 2005; Liu et al., 2015) and we observed a significant inhibition of translation in neurons exposed to APOE4 (Fig. 1). Hence, we aimed to investigate whether the NMDAR-mediated protein synthesis response is affected in the presence of APOE4. The activity of NMDARs has a very important role in synaptic plasticity. NMDAR stimulation leads to a distinct translation response which initially involves an inhibition of global translation with a small subset of mRNAs being translationally upregulated, followed by a more robust translation activation at a later phase (Kute et al., 2019; Ghosh Dastidar et al., 2020; Kuzniewska et al., 2020). Stimulation of cortical neurons with 20 μM NMDA for 5 min led to an increase in phosphorylation of eEF2 as previously reported (Kute et al., 2019; Ghosh Dastidar et al., 2020; Fig. 3*B*), indicating global translation inhibition. In this background of global translation inhibition, certain specific candidates such as PTEN and PSD95 are translationally activated (Kute et al., 2019). Consequently, we observed an increase in the protein levels of PTEN (Fig. 3*C*) and PSD95 (Fig. 3*D*) with our stimulation paradigm in the neurons, representing a NMDAR-specific translation response.

To test the effect of APOE treatment on NMDAR-mediated translation response, we incubated rat primary cortical neurons with APOE KO or APOE3 or APOE4 iPSC conditioned media (for biochemistry experiments) or recombinant protein (for FUNCAT experiments) for 20 min as previously described. During the last 5 min, the neurons were stimulated with 20 μM NMDA, followed by different assays to study the translation response (Fig. 3*A*). When we incubated the neurons with APOE KO conditioned media for 20 min, the translation response to NMDAR stimulation was unaffected; we observed an increase in eEF2 phosphorylation (Fig. 3*E*), PTEN protein levels (Fig. 3*F*) and PSD95 protein levels (Fig. 3*G*). NMDAR stimulation of the APOE3 conditioned media-treated neurons showed a similar increase in the phosphorylation of eEF2 indicating a normal NMDAR response (Fig. 3*H*). On the other hand, neurons exposed to APOE4 conditioned media did not show an increase in the phosphorylation of eEF2 on NMDAR stimulation (Fig.

←

primary cortical neurons (DIV15) were stimulated with 20 μM NMDA for 5 min, subjected to polysome profiling and probed for the distribution of ribosomal protein RPLP0. The immunoblots indicate the distribution of RPLP0 in the individual fractions. ***G***, The line graph indicates the percentage distribution of RPLP0 in the individual fractions under basal and 5-min NMDA stimulated conditions. ***H***, The graph represents the ratio of RPLP0 protein distribution in fractions 7–11 (translating pool) to fractions 1–6 (non-translating pool) under basal and 5-min NMDA stimulated conditions. Data are represented as mean ± SEM, $N = 3$, unpaired Student's t test. ***I***, Rat primary cortical neurons (DIV15) were treated with APOE3/APOE4 (10–15 nM) conditioned media for 20 min along with NMDAR stimulation for 5 min (20 μM NMDA). The cell lysates were subjected to polysome profiling and probed for the distribution of ribosomal protein RPLP0. The immunoblots show the distribution of RPLP0 in the individual fractions under different treatment conditions. ***J***, The line graph represents the percentage distribution of RPLP0 protein in fractions 4–11 under different APOE treatment conditions. ***K***, The graph represents the ratio of RPLP0 protein distribution in fractions 7–11 (translating pool) to fractions 1–6 (non-translating pool) under different APOE treatment conditions. Data are represented as mean ± SEM, $N = 3$, one-way ANOVA ($p = 0.0002$) followed by Tukey's multiple comparison test. ***L***, The line graph represents the percentage distribution of PTEN mRNA in each fraction under different APOE treatment conditions. ***M***, The graph represents the ratio of PTEN mRNA distribution in fractions 7–11 (translating pool) to fractions 1–6 (non-translating pool). Data are represented as mean ± SEM, $N = 3$, one-way ANOVA ($p = 0.006$) followed by Dunnett's multiple comparison test, ns in the figure implies non-significant. ***N***, The line graph represents the percentage distribution of PSD95 mRNA in each fraction under different APOE treatment conditions. ***O***, The graph represents the ratio of PSD95 mRNA distribution in fractions 7–11 (translating pool) to fractions 1–6 (non-translating pool). Data are represented as mean ± SEM, $N = 3$, one-way ANOVA ($p = 0.0286$) followed by Dunnett's multiple comparison test, ns in the figure implies non-significant. ***P***, The line graph represents the percentage distribution of β-actin mRNA in each fraction under different APOE treatment conditions. ***Q***, The graph represents the ratio of β-actin mRNA distribution in fractions 7–11 (translating pool) to fractions 1–6 (non-translating pool). Data are represented as mean ± SEM, $N = 3$, one-way ANOVA (ns - non-significant). ***R***, The line graph represents the percentage distribution of α-tubulin mRNA in each fraction under different APOE treatment conditions. ***S***, The graph represents the ratio of α-tubulin mRNA distribution in fractions 7–11 (translating pool) to fractions 1–6 (non-translating pool). Data are represented as mean ± SEM, $N = 3$, one-way ANOVA (ns - non-significant).

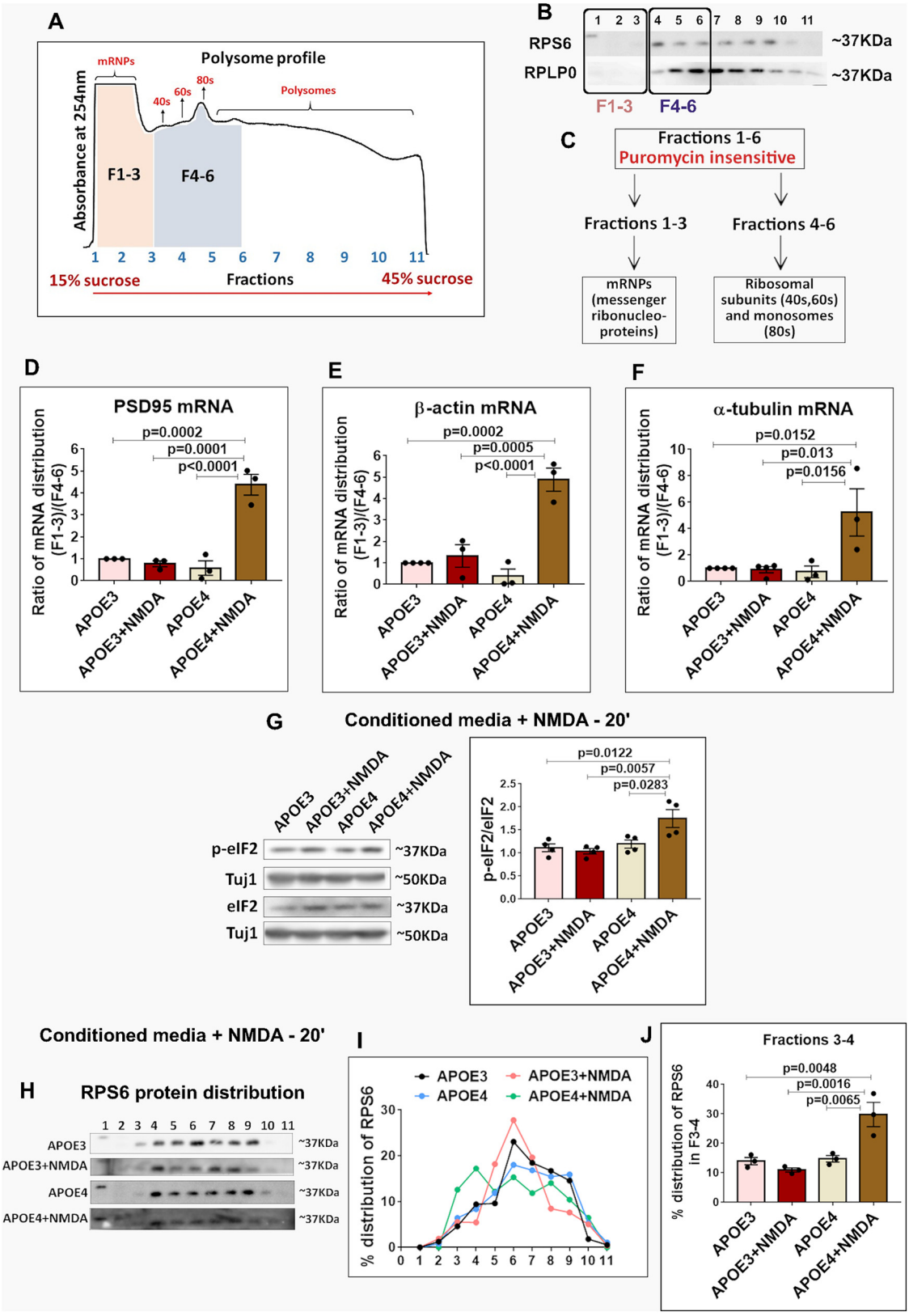

Figure 5. The NMDAR stimulation of APOE4-treated neurons invokes a stress response, potentially through inhibition of translation initiation and eIF2 phosphorylation. ***A***, Polysome profile indicating the fractions (F1–3 and F4–6) from the puromycin insensitive pool considered for the experiments and analysis. ***B***, Representative immunoblots of ribosomal protein RPS6 and RPLP0 highlighting the pools F1–3 (mRNPs) and F4–6 (40S, 60S and 80S) considered for the experiments and analysis. ***C***, Schematic showing division of puromycin insensitive fractions 1–6 into two pools: fractions 1–3 which constitute the mRNPs and fractions 4–6 which constitute the ribosomal subunits (40S, 60S) and monosomes (80S). ***D–F***, Rat primary cortical neurons (DIV15) were treated with APOE3/APOE4 (10–15 nM) conditioned media for 20 min along with NMDAR stimulation for 5 min (20 μM NMDA). The cell lysates were subjected to polysome profiling and probed for the distribution of the following candidate mRNAs in fractions 1–6 using RT-PCR method. ***D***, The graph represents the ratio of PSD95 mRNA distribution in fractions 1–3 to fractions 4–6. Data are represented as mean ± SEM, $N = 3$, one-way ANOVA ($p < 0.0001$) followed by Tukey's multiple comparison test. ***E***, The graph represents the ratio of β-actin mRNA

3*H*). However, it should be noted that APOE4 treatment alone caused an increase in eEF2 phosphorylation compared with APOE3-treated neurons, but APOE4-treated neurons failed to evoke the NMDAR-mediated increase in eEF2 phosphorylation (Fig. 3*H*). We have previously shown that NMDAR stimulation for 5 min causes a significant decrease in the total protein synthesis as measured by FUNCAT assay (Ghosh Dastidar et al., 2020). In the neurons treated with recombinant APOE3 protein, 5-min stimulation of NMDARs caused a decrease in the FUNCAT signal (Fig. 3*I*,*J*) indicating a normal NMDAR response. However, in the neurons exposed to recombinant APOE4 protein, the NMDA-induced decrease in the FUNCAT signal was completely lost (Fig. 3*I*,*J*). Again, APOE4 exposure alone caused a significant decrease in the FUNCAT signal and NMDAR stimulation failed to elicit a response in APOE4 background (Fig. 3*I*,*J*).

With respect to the NMDAR-specific translation activation, APOE3 conditioned media-treated neurons showed a significant increase in PTEN (Fig. 3*K*) and PSD95 (Fig. 3*L*) protein levels on 5-min NMDAR stimulation. But, in the presence of APOE4 conditioned media, the NMDAR-mediated increase in the levels of PTEN and PSD95 proteins were lost (Fig. 3*K*,*L*). Furthermore, there were elevated levels of PTEN and PSD95 proteins on APOE4 exposure alone, but the NMDAR-mediated increase was not observed. Since APOE4 has been previously reported to lead to transcriptional activation of several synaptic mRNAs (Huang et al., 2019), we checked whether PTEN and PSD95 mRNA levels were altered by APOE exposure. We did not observe any change in the mRNA levels of both PTEN (Fig. 3*M*) and PSD95 (Fig. 3*N*) with APOE KO, APOE3, and APOE4 iPSC conditioned media treatment for 20 min.

Finally, we also tested the NMDAR response in the presence of APOE in rat cortical synaptoneurosome preparations. When synaptoneurosomes were exposed to recombinant APOE3 protein for 20 min, they responded to NMDAR stimulation by showing an increase in eEF2 phosphorylation (Fig. 3*O*). But 20 min exposure to APOE4 recombinant protein resulted in a complete loss of the NMDAR response as there was no change in the phosphorylation of eEF2 (Fig. 3*P*). In summary, 20 min of exposure to APOE4 completely abolished the NMDAR-mediated translation response, both with respect to global translation inhibition and translation activation of specific candidates, whereas NMDAR response was unaffected by 20 min of APOE3 treatment. Interestingly, 20-min APOE4 treatment seemed to elicit a similar translation response as 5-min NMDAR stimulation, implying a role of NMDARs in the APOE4-mediated synaptic defect.

Aberrant translation response by APOE4 mimics the translation response on 5-min NMDAR stimulation

It was interesting that while 20 min of APOE4 exposure abolished the NMDAR-mediated translation response in neurons, APOE4 treatment alone mimicked the features of 5-min NMDAR translation response (Fig. 3). To further investigate this observation, we used the polysome profiling assay. We separated the rat primary cortical neuron lysate on a 15–45% linear sucrose gradient which was fractionated into 11 samples (Fig. 4*A*). We used puromycin treatment to identify the translationally active polysome fractions (Fig. 4*B*–*E*). Puromycin treatment disrupts the actively translating polysomes, as indicated by the absorbance profile at 254 nm (Fig. 4*B*) and the shift in the distribution of the ribosomal protein RPLP0 (Fig. 4*C*,*D*). The ribosomal fractions 7–11, which were disrupted by puromycin, were grouped as the actively translating pool (Fig. 4*C*–*E*), whereas fractions 1–6, which are insensitive to puromycin treatment, were grouped as the non-translating pool (Fig. 4*C*–*E*). After 5-min NMDAR stimulation of neurons, we observed an increase in eEF2 phosphorylation indicating global translation inhibition (Fig. 3). This global translation inhibition was also clearly reflected in the shift of ribosomes (RPLP0 protein) from the translationally active pool (fractions 7–11) to the inactive pool (fractions 1–6; Fig. 4*F*–*H*). A 20-min treatment with APOE3 conditioned media along with 5-min NMDAR stimulation showed the same response of ribosomal shift (RPLP0) toward the translationally inactive fractions (Fig. 4*I*–*K*), indicating that the exposure to APOE3 does not affect the NMDAR response. APOE4 conditioned media treatment for 20 min resulted in the shift of the ribosomes (RPLP0) into the translationally inactive fractions (Fig. 4*I*–*K*), similar to 5-min NMDAR stimulation in the APOE3 background. Interestingly, APOE4 treatment along with 5-min NMDAR stimulation caused a further and maximum shift of the ribosomes (RPLP0) from the translationally active fractions 7–11 toward the inactive fractions *1*–6 (Fig. 4*I*–*K*).

We have previously shown that, in the background of global inhibition of protein synthesis, NMDAR stimulation leads to translation activation of specific candidates such as PTEN and PSD95 (Fig. 3; Kute et al., 2019). We further investigated the distribution of PTEN and PSD95 mRNAs in the polysome fractions under APOE treatment conditions. On 5-min NMDAR stimulation in APOE3 background (20 min), we observed a shift of PTEN (Fig. 4*L*,*M*) and PSD95 (Fig. 4*N*,*O*) mRNAs into the translationally active polysome fractions, validating that the normal NMDAR response was intact in the background of APOE3. Conversely, PTEN (Fig. 4*L*,*M*) and PSD95 (Fig. 4*N*,*O*) mRNAs shifted to the translating pool with 20 min of APOE4 exposure, even without NMDAR stimulation. This reinforces the idea that 20 min of exposure to APOE4 brings about the same translation response as 5-min NMDAR stimulation. Additionally, NMDAR stimulation in the background of APOE4 elicited a very different response. It did not lead to the translation activation of PTEN and PSD95 mRNAs (Fig. 4*L*–*O*), although it caused a decrease of ribosomes from the translationally active pool compared with APOE4 treatment (Fig. 4*J*,*K*). β-Actin (Fig. 4*P*,*Q*) and α-tubulin (Fig. 4*R*,*S*) mRNAs were used as controls as their translation was unaffected by both NMDAR stimulation and APOE exposure. In summary, 20-min treatment with APOE4 caused a translation response which appeared to be similar to 5-min NMDAR

←

distribution in fractions 1–3 to fractions 4–6. Data are represented as mean ± SEM, $N = 3$, one-way ANOVA ($p < 0.0001$) followed by Tukey's multiple comparison test. ***F***, The graph represents the ratio of α-tubulin mRNA distribution in fractions 1–3 to fractions 4–6. Data are represented as mean ± SEM, $N = 3$–4, one-way ANOVA ($p = 0.0079$) followed by Tukey's multiple comparison test. ***G***, Rat primary cortical neurons (DIV15) were treated with APOE3/APOE4 (10–15 nM) conditioned media for 20 min along with NMDAR stimulation for 5 min (20 μM NMDA) and probed for phosphorylation of eIF2α. Left, Representative immunoblots indicating levels of phospho-eIF2α, eIF2α, and Tuj1. Right, Graph indicating ratio of phospho-eIF2 to eIF2 normalized to Tuj1. Data are represented as mean ± SEM, $N = 4$, one-way ANOVA ($p = 0.0047$) followed by Tukey's multiple comparison test. ***H***, Rat primary cortical neurons (DIV15) were treated with APOE3/APOE4 (10–15 nM) conditioned media for 20 min along with NMDAR stimulation for 5 min (20 μM NMDA). The cell lysates were subjected to polysome profiling and probed for the ribosomal protein RPS6. The immunoblots show the distribution of RPS6 on the linear sucrose gradient under different conditions. ***I***, The line graph represents the percentage distribution of RPS6 protein in each fraction under different APOE treatment conditions. ***J***, The graph represents the percentage distribution of RPS6 protein in fractions 3–4 under different APOE treatment conditions. Data are represented as mean ± SEM, $N = 3$, one-way ANOVA ($p = 0.0015$) followed by Tukey's multiple comparison test.

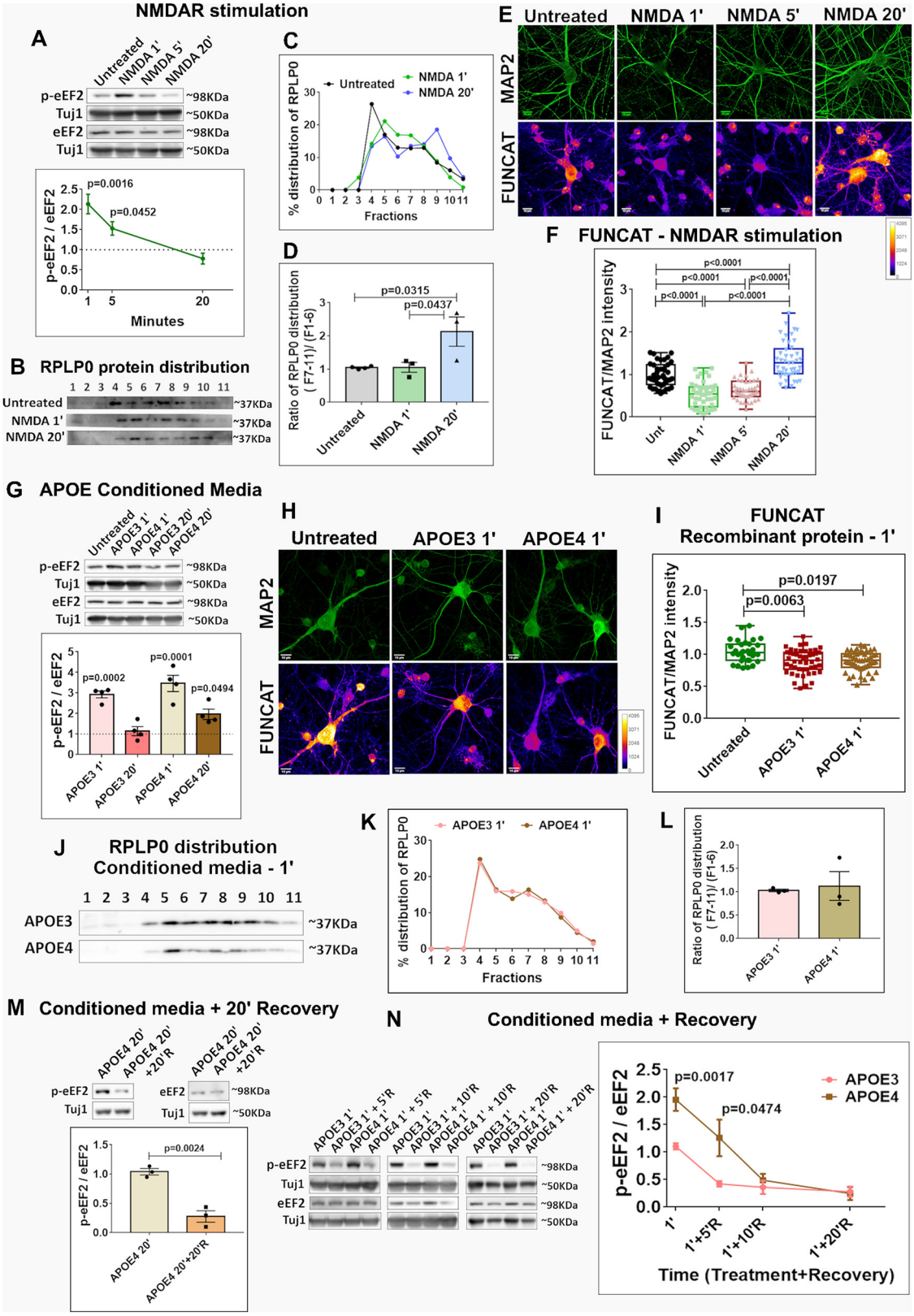

Figure 6. Temporal profiles of NMDA, APOE3, and APOE4 translation response. ***A***, Rat primary cortical neurons (DIV15) were treated with NMDA (20 μM) for 1, 5, and 20 min and probed for phosphorylation of eEF2. Top, Representative immunoblots indicating levels of phospho-eEF2, eEF2, and Tuj1. Bottom, Graph indicating ratio of phospho-eEF2 to eEF2 normalized to Tuj1. Data are represented as mean ± SEM, $N = 3$, one-way ANOVA ($p = 0.0015$) followed by Tukey's multiple comparison test. ***B***, Rat primary cortical neurons (DIV15) were stimulated with 20 μM NMDA for 1 and 20 min, subjected to polysome profiling and probed for the distribution of ribosomal protein RPLP0. The immunoblots indicate the distribution of RPLP0 in the individual fractions. ***C***, Line graph showing the percentage distribution of RPLP0 under different NMDA stimulation conditions. ***D***, Bar graph representing the ratio of RPLP0 protein distribution in fractions 7–11 (translating pool) to fractions 1–6 (non-translating pool) under different NMDA stimulation conditions. Data are represented as mean ± SEM, $N = 3$, one-way ANOVA ($p = 0.0248$) followed by Tukey's multiple comparison test. ***E***, Rat primary cortical neurons (DIV15) were stimulated with NMDA (20 μM) for 1, 5, and 20 min and subjected to FUNCAT along with

stimulation in APOE3 background. However, NMDAR stimulation in the background of APOE4 resulted in an aberrant translation response.

NMDAR stimulation in the background of APOE4 causes a stress response

Following 20-min treatment with APOE4, neurons lost the ability to respond to NMDAR stimulation while similar exposure to APOE3 had no such effect (Figs. 3, 4). In the polysome profiling assay, we observed that the shift of ribosomes into the translationally inactive pool was highest in the neurons stimulated with NMDA in the background of APOE4 treatment (Fig. 4*J*,*K*). To understand this phenomenon better, we further analyzed only the puromycin insensitive fractions (fractions 1–6) to study the redistribution of the mRNAs within this pool (Fig. 5*A*). Within this pool, fractions 4–6 showed a signal for the ribosomal proteins RPLP0 (large subunit) or RPS6 (small subunit) or both indicating that these fractions contain either ribosomal subunits or monosomes (Fig. 5*B*,*C*), as reflected in the absorbance profile at 254nm as well (Fig. 5*A*). Fractions 1–3, which did not show any signal for ribosomal proteins, were mainly enriched in the messenger ribonucleoproteins (mRNPs) representing the mRNAs that are not associated with the ribosomes (Fig. 5*B*,*C*).

When we investigated the redistribution of the mRNAs between mRNP fractions (fractions 1–3) and ribosomal fractions (fractions 4–6) on NMDAR stimulation, we did not observe any significant change in the APOE3 background, while there was a 3- to 5-fold increase of mRNAs in the mRNP fractions in the APOE4 background (Fig. 5*D*–*F*). While NMDAR-mediated translation activation was specific only to a subset of mRNAs, there was no such specificity in the NMDA-induced shift of mRNAs into the mRNP fractions in the APOE4 background. Even the mRNAs such as β-actin and α-tubulin, which did not respond to NMDAR stimulation in the APOE3 background, were shifted to mRNP fractions in the APOE4 background (Fig. 5*E*,*F*). This was an aberrant response that was consistent with stress-induced global translation inhibition.

To verify whether this was a stress response, we probed into the phosphorylation status of eukaryotic translation initiation factor eIF2α, a well-established marker for stress (Richter and Klann, 2009; Pakos-Zebrucka et al., 2016), which has been implicated in AD pathology as well (Ma et al., 2013). APOE3 conditioned media treatment (20 min) along with 5-min NMDAR stimulation did not cause a change in the phosphorylation of eIF2α (Fig. 5*G*), while it increased eEF2 phosphorylation (Fig. 3). But, in the presence of APOE4 conditioned media (20 min), 5-min NMDAR stimulation caused a significant increase in eIF2α phosphorylation (Fig. 5*G*), while there was no change in eEF2 phosphorylation (Fig. 3). Additionally, NMDAR stimulation in the background of APOE4 caused a clear shift of the ribosomal protein RPS6 (small subunit) into fractions 3–4 (Fig. 5*H*–*J*), which likely represents the unassembled subunits of the ribosome. The accumulation of the small subunit of the ribosome indicated an increased inhibition of translation at the initiation step, which was another characteristic feature of the stress response. We did not observe such a shift of RPS6 on NMDAR stimulation in the APOE3 background (Fig. 5*H*–*J*). Overall, these results indicated that NMDAR stimulation of APOE4-treated neurons potentially leads to a pathologic stress response.

Translation response elicited by APOE treatment and NMDAR stimulation are different temporally

An important feature of synaptic activity mediated translation is its unique spatial and temporal pattern of regulation (Ghosh Dastidar et al., 2020). NMDAR-mediated translation response is a good example of this. Initially, NMDAR stimulation leads to global translation inhibition which gradually changes to a phase of robust translation activation (Ghosh Dastidar et al., 2020). We were able to capture this temporal pattern of NMDAR-mediated translation response using the phosphorylation status of eEF2 as one of the readouts (Fig. 6*A*). On NMDAR stimulation (20 μM NMDA) of cultured cortical neurons, we observed a rapid and robust 2-fold increase in the phosphorylation of eEF2 at 1 min. By 5 min, the phosphorylation of eEF2 was reduced, but it remained significantly high (1.5-fold increase) compared with the untreated/basal condition (Fig. 6*A*). By 20 min, the phosphorylation of eEF2 was further reduced below the basal/untreated level (<1.0) indicating global translation activation (Fig. 6*A*). This temporal pattern of translation was also reflected in the polysome profiling assay and RPLP0 distribution (Fig. 6*B*–*D*). Stimulation with NMDA (20 μM) for 1 min did not cause any change in the shift of ribosomes (RPLP0 distribution; Fig. 6*B*–*D*). However, 20-min NMDAR stimulation caused an increase in the heavier polysomes and a significant shift of RPLP0 toward the translating fractions 7–11, clearly indicating translation activation (Fig. 6*B*–*D*). We further validated the temporal translation profile by performing the FUNCAT assay with 1 min, 5- and 20-

←

immunostaining for MAP2. The representative images for MAP2 and FUNCAT fluorescent signal under different treatment conditions are shown (scale bar: 10 μm). ***F***, The graph represents the quantification of the FUNCAT fluorescent intensity normalized to MAP2 fluorescent intensity under different NMDAR stimulation time points. Each data point represents an individual neuron. $N = 40–50$ neurons from 3 independent experiments, one-way ANOVA ($p < 0.0001$) followed by Tukey's multiple comparison test. ***G***, Rat primary cortical neurons (DIV15) were treated with APOE3/APOE4 (10–15 nM) conditioned media for 1 and 20 min and probed for the phosphorylation of eEF2. Top, Representative immunoblots indicating levels of phospho-eEF2, eEF2, and Tuj1. Bottom, Graph indicating ratio of phospho-eEF2 to eEF2 normalized to Tuj1. Data are represented as mean ± SEM. Dotted line indicates the untreated condition. All the APOE treatments were normalized to untreated condition; $N = 4$, one-way ANOVA ($p < 0.0001$) followed by Dunnett's multiple comparison test. ***H***, Rat primary cortical neurons (DIV15) were treated with recombinant APOE protein (15 nM) for 1 min and subjected to FUNCAT along with immunostaining for MAP2. The representative images for MAP2 and FUNCAT fluorescent signal under different APOE treatment conditions are shown (scale bar: 10 μm). ***I***, The graph represents the quantification of the FUNCAT fluorescent intensity normalized to MAP2 fluorescent intensity under different APOE treatment conditions. Each data point represents an individual neuron. $N = 20–40$ neurons from 4 independent experiments, one-way ANOVA ($p = 0.0058$) followed by Tukey's multiple comparison test. ***J***, Rat primary cortical neurons (DIV15) were treated with APOE3/APOE4 conditioned media (10–15 nM) for 1 min, subjected to polysome profiling and probed for the distribution of ribosomal protein RPLP0. The immunoblots indicate the distribution of RPLP0 in the individual fractions. ***K***, The line graph shows the percentage distribution of RPLP0 under different APOE treatment conditions. ***L***, The bar graph represents the ratio of RPLP0 protein distribution in fractions 7–11 (translating pool) to fractions 1–6 (non-translating pool) under different APOE treatment conditions. Data are represented as mean ± SEM, $N = 3$, unpaired Student's *t* test (ns - non-significant). ***M***, Rat primary cortical neurons (DIV15) were treated with APOE4 (10–15 nM) conditioned media for 20 min and subjected to recovery for 20 min using preconditioned neurobasal media. The samples were probed for the phosphorylation of eEF2. Top, Representative immunoblots indicating levels of phospho-eEF2, eEF2, and Tuj1. Bottom, Graph indicating ratio of phospho-eEF2 to eEF2 normalized to Tuj1. Data are represented as mean ± SEM, $N = 3$, unpaired Student's *t* test. ***N***, Rat primary cortical neurons (DIV15) were treated with APOE3/APOE4 (10–15 nM) conditioned media for 1 min and subjected to recovery for 5/10/20 min using preconditioned neurobasal media, and probed for the phosphorylation of eEF2. The data from each recovery time point are normalized to its corresponding 1-min APOE-treated set. Left, Representative immunoblots indicating levels of phospho-eEF2, eEF2, and Tuj1. Right, Graph indicating ratio of phospho-eEF2 to eEF2 normalized to Tuj1. Data are represented as mean ± SEM. For APOE3 1′ and APOE4 1′, $N = 8$, unpaired Student's *t* test. For APOE 1′ + 5′R, $N = 4$, unpaired Student's *t* test. For APOE 1′ + 10′R, $N = 5$. For APOE 1′ + 20′R, $N = 3$.

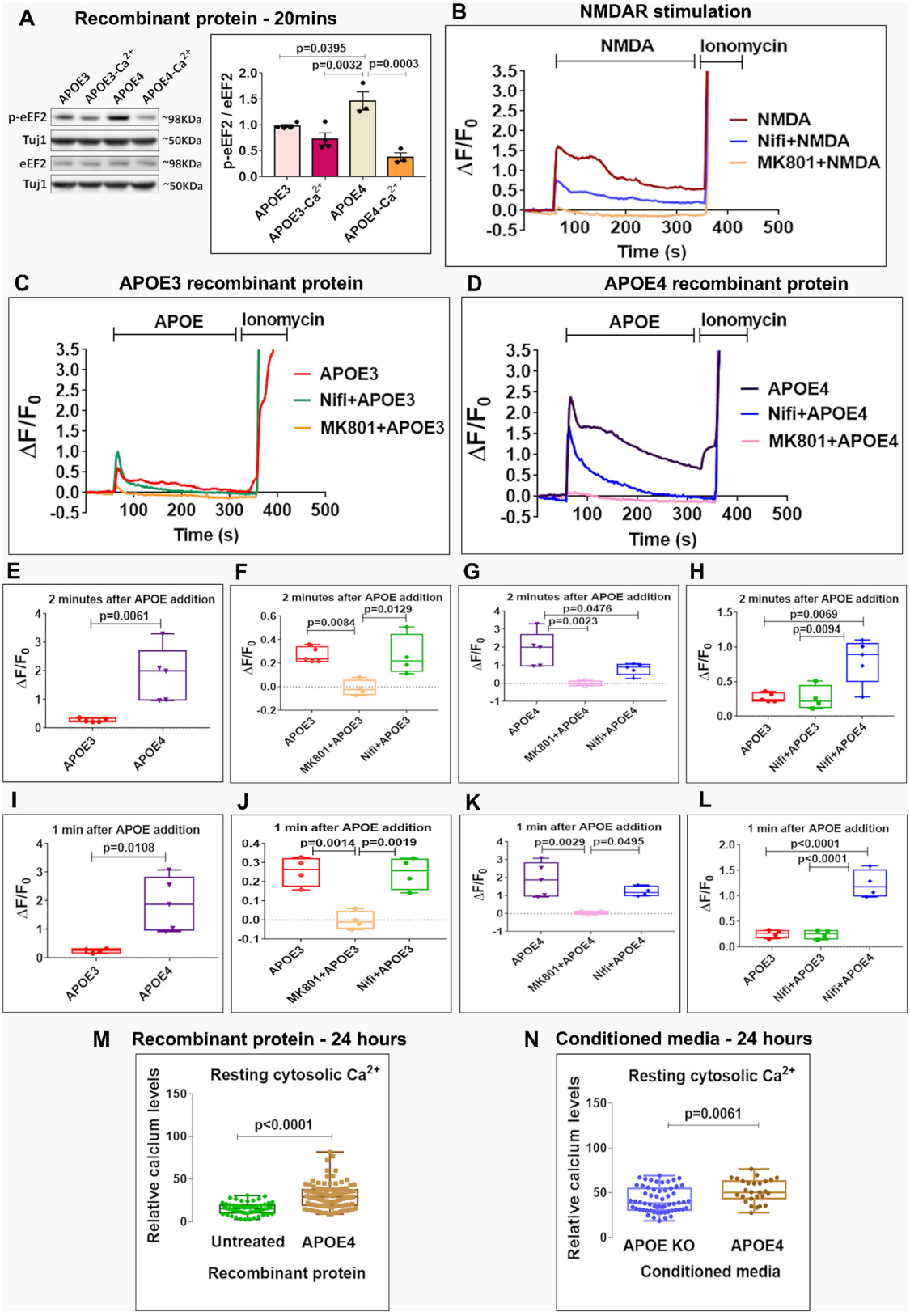

Figure 7. The distinct calcium signatures generated by NMDAR stimulation, APOE3 treatment and APOE4 treatment. ***A***, Rat primary cortical neurons (DIV15) were treated with recombinant APOE3/APOE4 protein (15 nM) for 20 min in the presence or absence of extracellular calcium (ACSF with or without calcium) and probed for the phosphorylation of eEF2. Left, Representative immunoblots indicating levels of phospho-eEF2, eEF2, and Tuj1. Right, Graph indicating ratio of phospho-eEF2 to eEF2 normalized to Tuj1. Data are represented as mean ± SEM, $N = 3–4$, one-way ANOVA ($p = 0.0004$) followed by Tukey's multiple comparison test. ***B–D***, Rat primary cortical neurons (DIV15) were subjected to calcium imaging for 5 min. The graphs represent the time trace for the change in Flou4-AM fluorescence compared with initial fluorescence (ΔF/F0) under the following conditions. ***B***, NMDAR stimulation (20 μM), nifedipine (50 μM) pretreatment followed by NMDAR stimulation (20 μM), and MK801 (25 μM) pretreatment followed by NMDAR stimulation (20 μM). ***C***, APOE3 treatment (15 nM), nifedipine (50 μM) pretreatment followed by APOE3 addition (15 nM), and MK801 (25 μM) pretreatment followed by APOE3 addition (15 nM). ***D***, APOE4 treatment (15 nM), nifedipine (50 μM) pretreatment followed by APOE4 addition (15

min NMDAR stimulation paradigms in the primary cortical neurons (Fig. 6*E*,*F*). As observed earlier, 1- and 5-min NMDAR stimulation caused a significant reduction in the FUNCAT signal indicating translation inhibition (Fig. 6*E*,*F*). However, 20-min NMDAR stimulation caused a robust increase in the FUNCAT signal compared with all the time points depicting the phase of global translation activation (Fig. 6*E*,*F*).

In the previous sections, we have shown that the exposure to APOE4, but not APOE3, for 20 min generated a translation response similar to 5-min NMDAR stimulation (Figs. 3, 4). For a more comprehensive understanding of the effect of APOE in comparison to NMDAR stimulation, we studied the effect of APOE3 and APOE4 on neuronal translation at both 1- and 20-min time points. Interestingly, with 1-min conditioned media treatment, unlike the 20-min time point, both APOE3 and APOE4 showed a significant increase in eEF2 phosphorylation (Fig. 6*G*). There was also a significant decrease in the FUNCAT signal in neurons exposed to recombinant APOE3 and APOE4 for 1 min (Fig. 6*H*,*I*). These results indicated that, at the 1-min time point, both APOE3 and APOE4 elicited a translation response that resembled NMDAR stimulation. The key difference was at the 20-min time point. On 20-min NMDAR stimulation, the phosphorylation of eEF2 was below the basal level (~1.35-fold) indicating translation activation (Fig. 6*A*). In the case of APOE3 treatment, the phosphorylation of eEF2 was back to basal level by 20 min (Fig. 6*G*). With APOE4 exposure, although eEF2 phosphorylation at 20 min was lower than the 1-min time point, it was still significantly higher (1.5-fold) than the basal level (Fig. 6*G*). There was no difference in the ribosomal (RPLP0) distribution between APOE3 and APOE4 conditioned media-treated neurons at 1 min (Fig. 6*J*–*L*), unlike the 20-min time point where APOE4-treated neurons showed a shift of ribosomes to the non-translating fractions (Fig. 4). This indicated that the recovery from the translation inhibition could be different between APOE3 and APOE4 treatments.

Since the brain has elaborate mechanisms to clear APOE, we wanted to study how the neurons recover from APOE exposure. To understand this, we added a 20-min recovery period following 20-min APOE4 conditioned media exposure. When we tested the neurons after 20 min of recovery, phosphorylation of eEF2 was significantly reduced (Fig. 6*M*), implying that the APOE4-mediated effect could be recovered. To further study the rate of recovery and their differences between the APOE isoforms, we treated the neurons with either APOE3 or APOE4 conditioned media for 1 min (a time point where both APOE3 and APOE4 induced a robust translation inhibition; Fig. 6*G*–*I*), followed by a recovery of 5, 10, and 20 min (Fig. 6*N*). Interestingly, with 1-min treatment followed by 5 min of recovery, the phosphorylation of eEF2 was still significantly higher in neurons exposed to APOE4 compared with APOE3 (Fig. 6*N*). But, by 10 and 20 min of recovery, both APOE3-treated and APOE4-treated neurons had reached the same level of eEF2 phosphorylation, indicating that the rate of recovery from translation inhibition was significantly slower in APOE4-treated neurons (Fig. 6*N*). In summary, while both APOE3 and APOE4 induced a robust translation inhibition at 1 min similar to NMDAR stimulation, their responses followed different temporal trajectories. The recovery from translation inhibition was slower in APOE4-treated neurons indicating the involvement of additional components in the APOE4-induced response.

The translation response of APOE and NMDARs are closely linked to their calcium signature

An important feature of APOE4-induced translation inhibition was that it resembled the NMDAR stimulation but also abolished the actual NMDAR-mediated response. Since the NMDAR translation response is primarily because of the influx of calcium into the neurons (Ghosh Dastidar et al., 2020), we tested the effect of extracellular calcium in the APOE4-induced translation response. We treated the neurons with recombinant APOE3 or APOE4 protein for 20 min in ACSF medium with or without calcium (Fig. 7*A*). As shown in the previous figures, incubation with APOE4 recombinant protein for 20 min resulted in a significant increase in eEF2 phosphorylation when compared with APOE3 treatment (Fig. 7*A*), but the absence of calcium in the media abolished the APOE4-induced increase in the phosphorylation of eEF2 (Fig. 7*A*). Although the absence of calcium showed a trend of decrease in eEF2 phosphorylation in the presence of APOE3 as well, it was not significant (Fig. 7*A*). Thus, calcium influx had an important role in APOE4-mediated translation inhibition. Hence, we wanted to understand the calcium profiles of APOE3 and APOE4, and also compare it to the calcium profile of NMDAR stimulation. To study this, we measured the changes in cytosolic calcium in neurons on NMDA or APOE addition for 5 min using Fluo4-AM dye.

On NMDAR stimulation, there was a rapid influx of calcium and the increase in cytosolic calcium levels was sustained for 5 min (Fig. 7*B*). NMDAR antagonist MK801 completely abolished NMDAR-mediated calcium influx (Fig. 7*B*), confirming the specificity of the response. It was previously reported that L-VGCCs are essential for the sustenance of NMDAR-mediated calcium (Dittmer et al., 2017). Inhibition of L-VGCCs using nifedipine did not block the influx of calcium on NMDAR stimulation, but it eliminated the latter part of the sustained calcium response (Fig. 7*B*). This verified that L-VGCCs were an important contributor to NMDAR-induced calcium influx. The addition of recombinant APOE3 protein led to a small burst of calcium (Fig. 7*C*), whereas the addition of recombinant APOE4 protein caused a robust and sustained increase in the cytosolic calcium which was substantially larger than APOE3 (Fig. 7*C*,*D*). The change in the fluorescent intensity calculated after APOE addition also showed that APOE4 caused a significant increase in calcium levels compared with APOE3, both at the 1- and 2-min time point (Fig. 7*E*,*I*). MK801 treatment abolished the calcium influx for both APOE3 and APOE4 addition (Fig. 7*C*,*D*), indicating that NMDARs were the primary source of calcium.

←

nM), and MK801 (25 μM) pretreatment followed by APOE4 addition (15 nM). ***E–H***, Box plots represent the quantification of the change in Flou4-AM fluorescence (ΔF/F0) after 2 min of APOE addition. $N = 4–5$ experiments, each experiment has the average value of 40–50 neurons. ***E***, Unpaired Student's *t* test. ***F***, One-way ANOVA ($p = 0.0058$) followed by Tukey's multiple comparison test. ***G***, One-way ANOVA ($p = 0.0029$) followed by Tukey's multiple comparison test. ***H***, One-way ANOVA ($p = 0.0038$) followed by Tukey's multiple comparison test. ***I–L***, Box plots represent the quantification of the change in Flou4-AM fluorescence (ΔF/F0) after 1 min of APOE addition. $N = 4–5$ experiments, each experiment has the average value of 40–50 neurons. ***I***, Unpaired Student's *t* test. ***J***, One-way ANOVA ($p = 0.0008$) followed by Tukey's multiple comparison test. ***K***, One-way ANOVA ($p = 0.0038$) followed by Tukey's multiple comparison test. ***L***, One-way ANOVA ($p < 0.0001$) followed by Tukey's multiple comparison test. ***M***, Rat primary cortical neurons (DIV15) were treated with APOE4 recombinant protein (15 nM) for 24 h and subjected to calcium imaging using Fluo8-AM. The graph shows the resting cytosolic calcium measured in these neurons. $N = 50–60$ neurons from 3 independent experiments. Kolmogorov–Smirnov test. ***N***, Rat primary cortical neurons (DIV15) were treated with APOE KO or APOE4 (10–15 nM) conditioned media for 24 h and subjected to calcium imaging using Fluo8-AM. The graph shows the resting cytosolic calcium measured in these neurons. $N = 50–60$ neurons from 3 independent experiments. Kolmogorov–Smirnov test.

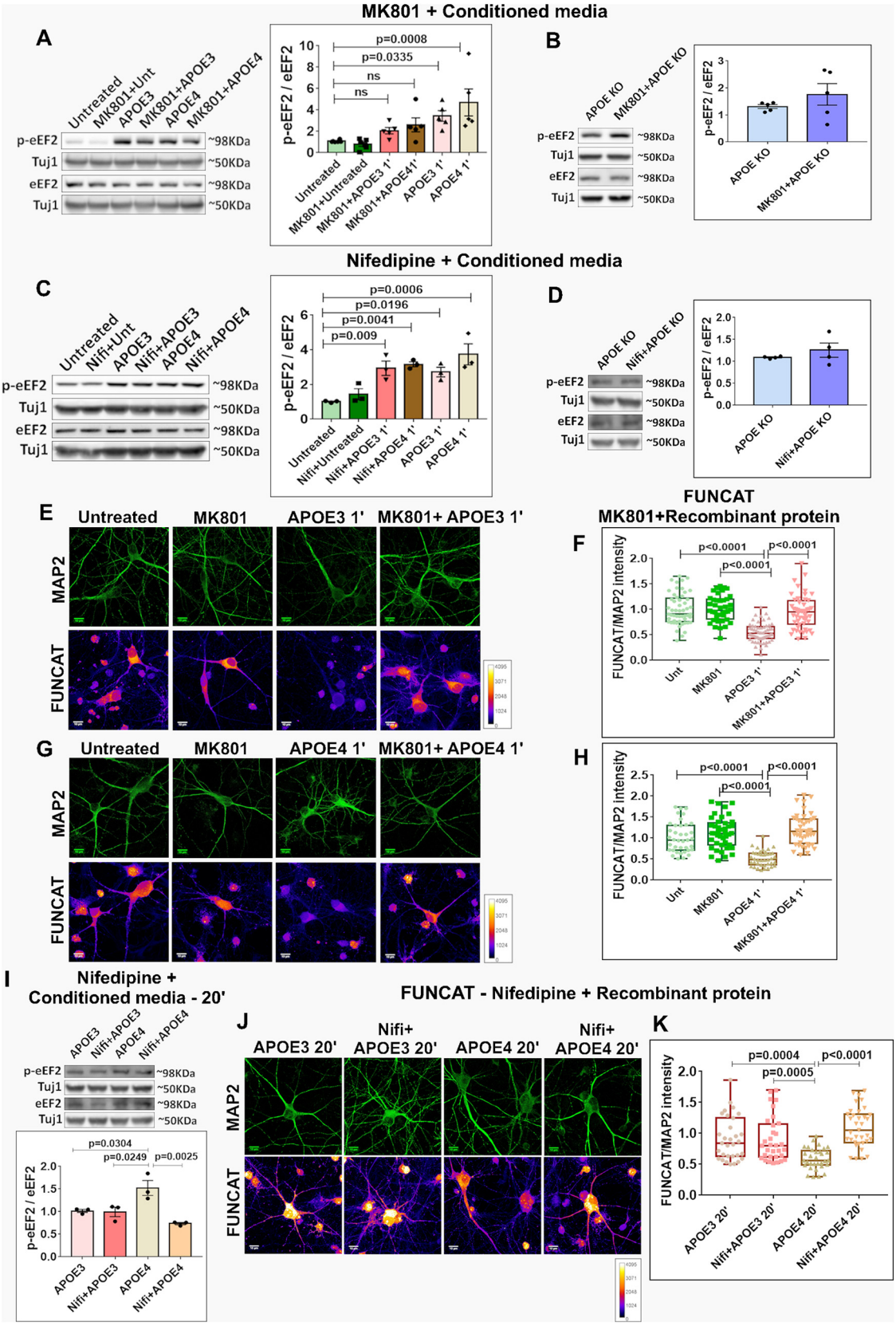

Figure 8. The APOE-mediated translation response is regulated by calcium signature and its sources. ***A***, Rat primary cortical neurons (DIV15) were treated with MK801 (25 μM) along with APOE3 or APOE4 (10–15 nM) conditioned media for 1 min and probed for phosphorylation of eEF2. Left, Representative immunoblots indicating levels of phospho-eEF2, eEF2, and Tuj1. Right, Graph indicating ratio of phospho-eEF2 to eEF2 normalized to Tuj1. Data are represented as mean ± SEM, $N = 5$, one-way ANOVA ($p = 0.0006$) followed by Dunnett's multiple comparison test. ***B***, Rat primary cortical neurons (DIV15) were treated with MK801 (25 μM) along with APOE KO conditioned media for 1 min and probed for the phosphorylation of eEF2. Left, Representative immunoblots indicating levels of phospho-eEF2, eEF2, and Tuj1. Right, Graph indicating ratio of phospho-eEF2 to eEF2 normalized to Tuj1. Data are represented as mean ± SEM, $N = 5$. Unpaired Student's t test (ns - non-significant). ***C***, Rat primary cortical neurons (DIV15) were treated with nifedipine (50 μM) along with APOE3 or APOE4 (10–15 nM) conditioned

Interestingly, treatment with L-VGCC-specific inhibitor nifedipine prevented the APOE4-mediated sustenance of calcium while it did not affect the APOE3-mediated calcium response (Fig. 7*C*,*D*). This indicated that APOE4 exposure caused a sustained increase in cytosolic calcium levels, which was initiated by calcium through NMDARs but the latter part of sustenance was primarily contributed by L-VGCCs.

Further quantification of the change in fluorescent intensities showed that APOE3 exposure led to a small increase in the cytosolic calcium which was prevented by MK801 both at 1- and 2-min time points; but nifedipine had no effect on APOE3-mediated calcium response at either of the time points (Fig. 7*F*,*J*). This showed that the APOE3 calcium response was mediated by NMDARs only. In case of APOE4, while nifedipine pretreatment reduced the calcium influx on APOE4 addition at 1 min, it was still significantly higher compared with MK801 pretreatment (Fig. 7*K*). But, by the 2-min time point, nifedipine also significantly reduced the APOE4-mediated calcium levels (Fig. 7*G*). This indicated that the contribution of L-VGCCs was substantial for the APOE4-mediated calcium response, particularly from 2 min onwards, rather than the earlier 1-min time point. Finally, even in the presence of nifedipine, the increase in cytosolic calcium levels caused by APOE4 was significantly higher than APOE3 both at 1 and 2 min, indicating that the initial NMDAR component was also higher in the case of APOE4 (Fig. 7*H*,*L*). In summary, both APOE3 and APOE4 caused initial calcium influx through NMDARs, but the extent of NMDAR-mediated calcium entry was higher in the case of APOE4. At a later phase, APOE4 also caused an influx of calcium through L-VGCCs which did not happen in the case of APOE3. We also observed that the chronic exposure (24 h) of APOE4 in the form of recombinant protein (Fig. 7*M*) or conditioned media (Fig. 7*N*) led to a significant increase in the cytosolic calcium levels in neurons. This sustained calcium increase was likely to be the cause of aberrant translation inhibition and the loss of synaptic activity mediated translation response in APOE4-treated neurons.

Further, we established the link between the different sources of calcium and the translation response generated by APOE. We tested the effect of 1-min treatment of APOE3 and APOE4 conditioned media on eEF2 phosphorylation in the presence of MK801 (NMDAR inhibitor). As shown previously (Fig. 6), 1-min treatment of APOE3 or APOE4 conditioned media led to a significant increase in eEF2 phosphorylation (Fig. 8*A*). However, in the presence of MK801, the phosphorylation of eEF2 on 1 min exposure to APOE3 and APOE4 was not significantly different from the untreated neurons (Fig. 8*A*). This indicated that at 1-min time point, both APOE3-mediated and APOE4-mediated translation inhibition was caused by the influx of calcium through NMDARs. Since we observed that the later part of APOE4-mediated calcium was through L-VGCCs, we tested whether blocking L-VGCCs would rescue the translation defect caused by APOE4. Preincubation of neurons with nifedipine (L-VGCC inhibitor) did not have any effect on the APOE3-induced or APOE4-induced translation response at 1 min, as measured by the phosphorylation of eEF2 (Fig. 8*C*). This corroborated the findings that L-VGCCs did not contribute to the APOE3 calcium response, and L-VGCCs did not have a role in the APOE4 calcium response at 1 min. MK801 or nifedipine alone did not have any effect on eEF2 phosphorylation in neurons exposed to APOE KO conditioned media (Fig. 8*B*,*D*). To further validate the effect of calcium influx through NMDARs on APOE-mediated translation response at 1 min, we performed FUNCAT assay in the neurons pretreated with MK801. As observed previously, the neurons treated with recombinant APOE3 (Fig. 8*E*,*F*) or APOE4 (Fig. 8*G*,*H*) protein for 1 min showed a reduction in the FUNCAT signal, indicating an inhibition of translation. But, when the neurons were pretreated with MK801, APOE3 (Fig. 8*E*, *F*), or APOE4 (Fig. 8*G*,*H*), mediated reduction in the FUNCAT signal was recovered, further demonstrating that the calcium influx through NMDARs caused the APOE3/APOE4-mediated translation inhibition at 1 min. As a control, MK801 pretreatment in the absence of APOE exposure did not cause any change in the FUNCAT signal (Fig. 8*E*–*H*).

At the 20-min time point, APOE4 conditioned media treatment caused an increase in eEF2 phosphorylation compared with APOE3 exposure (Fig. 8*I*). The presence of nifedipine significantly reduced the APOE4-mediated increase in eEF2 phosphorylation (Fig. 8*I*). Similarly, 20-min treatment with recombinant APOE4 protein caused a significant reduction in the FUNCAT signal compared with APOE3 treatment (Fig. 8*J*,*K*). However, there was no reduction in the FUNCAT signal of the neurons treated with APOE4 in the presence of nifedipine (Fig. 8*J*,*K*), further confirming the role of L-VGCCs in the later part of the APOE4-mediated translation defect. Hence, the translation inhibition caused by APOE4 has an early phase contributed by calcium through NMDARs while the sustenance of this response was because of the calcium through L-VGCCs. The perturbation of calcium

←

media for 1 min and probed for phosphorylation of eEF2. Left, Representative immunoblots indicating levels of phospho-eEF2, eEF2, and Tuj1. Right, Graph indicating ratio of phospho-eEF2 to eEF2 normalized to Tuj1. Data are represented as mean ± SEM, $N = 3$, one-way ANOVA ($p = 0.001$) followed by Dunnett's multiple comparison test. ***D***, Rat primary cortical neurons (DIV15) were treated with nifedipine (50 μM) along with APOE KO conditioned media for 20 min and probed for phosphorylation of eEF2. Left, Representative immunoblots indicating levels of phospho-eEF2, eEF2, and Tuj1. Right, Graph indicating ratio of phospho-eEF2 to eEF2 normalized to Tuj1. Data are represented as mean ± SEM, $N = 4$. Unpaired Student's *t* test (ns - non-significant). ***E***, Rat primary cortical neurons (DIV15) were treated with MK801 (25 μM) along with recombinant APOE3 protein (15 nM) for 1 min. They were subjected to FUNCAT along with immunostaining for MAP2. The representative images for MAP2 and FUNCAT fluorescent signal under different treatment conditions are shown (scale bar: 10 μm). ***F***, The graph represents the quantification of the FUNCAT fluorescent intensity normalized to MAP2 fluorescent intensity under different APOE3 treatment conditions. Each data point represents an individual neuron. $N = 40$–50 neurons from 4 independent experiments, one-way ANOVA ($p < 0.0001$) followed by Tukey's multiple comparison test. ***G***, Rat primary cortical neurons (DIV15) were treated with MK801 (25 μM) along with recombinant APOE4 protein (15 nM) for 1 min. They were subjected to FUNCAT along with immunostaining for MAP2. The representative images for MAP2 and FUNCAT fluorescent signal under different treatment conditions are shown (scale bar: 10 μm). ***H***, The graph represents the quantification of the FUNCAT fluorescent intensity normalized to MAP2 fluorescent intensity under different APOE4 treatment conditions. Each data point represents an individual neuron. $N = 40$–50 neurons from 4 independent experiments, one-way ANOVA ($p < 0.0001$) followed by Tukey's multiple comparison test. ***I***, Rat primary cortical neurons (DIV15) were treated with nifedipine (50 μM) along with APOE3 or APOE4 (10–15 nM) conditioned media for 20 min and probed for phosphorylation of eEF2. Top, Representative immunoblots indicating levels of phospho-eEF2, eEF2, and Tuj1. Bottom, Graph indicating ratio of phospho-eEF2 to eEF2 normalized to Tuj1. Data are represented as mean ± SEM, $N = 3$, one-way ANOVA ($p = 0.0036$) followed by Tukey's multiple comparison test. ***J***, Rat primary cortical neurons (DIV15) were treated with nifedipine (50 μM) along with recombinant APOE3 or APOE4 protein (15 nM) for 20 min. They were subjected to FUNCAT along with immunostaining for MAP2. The representative images for MAP2 and FUNCAT fluorescent signal under different treatment conditions are shown (scale bar: 10 μm). ***K***, The graph represents the quantification of the FUNCAT fluorescent intensity normalized to MAP2 fluorescent intensity under different treatment conditions. Each data point represents an individual neuron. $N = 20$–30 neurons from 4 independent experiments, one-way ANOVA ($p < 0.0001$) followed by Tukey's multiple comparison test.

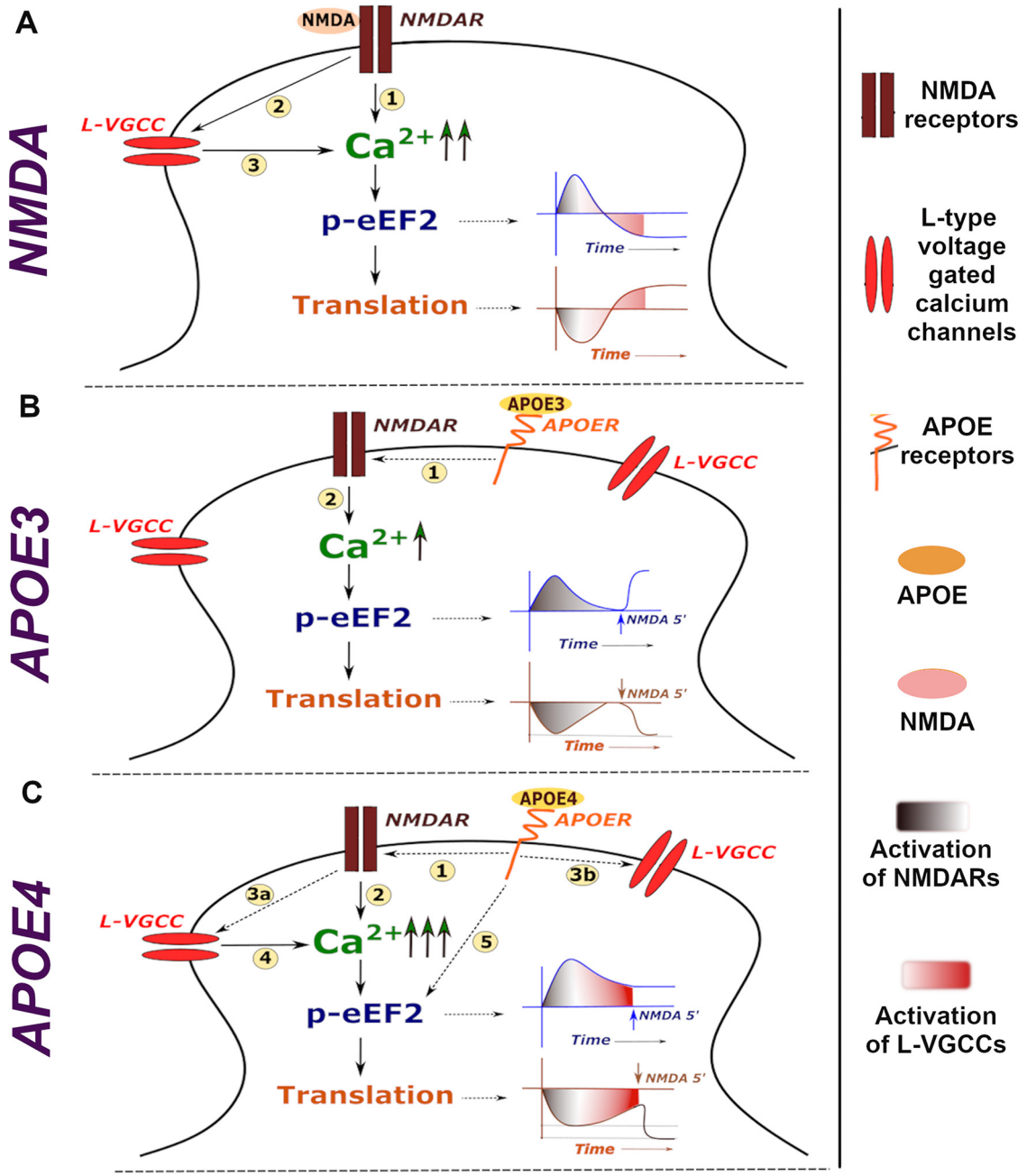

Figure 9. Model illustrating calcium signature and corresponding protein synthesis regulation downstream of NMDAR stimulation and APOE treatment. ***A***, Stimulation of NMDARs lead to influx of calcium through NMDARs (1) which activates L-VGCCs (2). The influx of calcium through L-VGCCs further helps in sustaining the calcium levels on NMDAR stimulation (3). The calcium through NMDARs and L-VGCCs generates a specific temporal profile of eEF2 phosphorylation, causing an initial inhibition of global protein synthesis followed by translation activation in a later phase. ***B***, Exposure to APOE3 activates NMDARs through an unknown mechanism (1), leading to a short burst of calcium through it (2). This leads to an acute increase in eEF2 phosphorylation, primarily contributed by calcium influx through NMDARs, which recovers to basal levels. Global translation also follows a similar temporal profile of initial decrease followed by recovery. Hence, the NMDA activity mediated translation response is unaffected in APOE3-treated neurons. ***C***, Exposure to APOE4 activates NMDARs through an unknown mechanism (1), causing higher influx of calcium through NMDARs (2) than APOE3 condition. The higher calcium influx through NMDARs could lead to L-VGCC activation in APOE4 condition (3a). Besides, APOE4 binding to APOE receptors could also directly regulate the sustained activation of L-VGCCs (3b). Overall, the L-VGCC activation under APOE4 treatment condition contributes to the huge and sustained increase in calcium levels (4). This leads to the sustained increase in eEF2 phosphorylation as well as global translation inhibition. There could also be a possibility of APOE4 activating signaling cascades which further contribute to the sustained increase in eEF2 phosphorylation (5). Hence, the NMDA activity mediated response is perturbed, potentially causing a stress-response phenotype in APOE4-treated neurons.

homeostasis disrupted the basal and NMDAR-mediated translation response in APOE4-treated neurons.

Discussion

In this study, we have shown that APOE4 inhibits protein synthesis in neurons and isolated synaptic compartments. We have tested this by using different sources of APOE, including APOE from stem cell conditioned media, astrocyte conditioned media, and recombinant protein. It is also important to note that we have used APOE at physiologically relevant low nanomolar concentrations (10 nM; Ulrich et al., 2013; Wang et al., 2018). An important aspect of our study was that we were able to identify the distinct temporal responses of protein synthesis generated by

APOE3 and APOE4. This gave us insights into how APOE3 and APOE4 lead to translation inhibition at 1 min and the key difference existed in their rate of recovery from the inhibition, where APOE4-mediated recovery was slower. The extent of eEF2 phosphorylation was another major difference between APOE3 and APOE4. Similar to the studies which show protein synthesis as an early defect in familial AD models (Ahmad et al., 2017; Cefaliello et al., 2020; Elder et al., 2020), our study raises the possibility of translation dysregulation as an early defect in APOE4-mediated pathology as well.

In neurons, the tight spatial and temporal regulation of synaptic translation is well studied for NMDAR stimulation (Scheetz et al., 2000; Hoeffer and Klann, 2008; Kute et al., 2019; Ghosh Dastidar et al., 2020). Initially, NMDAR stimulation leads to an inhibition of global protein synthesis which subsequently changes to a phase of translation activation (Kute et al., 2019; Ghosh Dastidar et al., 2020; Kuzniewska et al., 2020). The temporal changes in protein synthesis and correspondingly in the translatome would be important to promote the structural and functional changes at the synapse on NMDAR stimulation (Jiang and Schuman, 2002; Matsuzaki et al., 2004; Hunt and Castillo, 2012). The interesting finding was that both APOE3 and APOE4 treatment appeared to mimic the translation inhibition phase of NMDAR stimulation. While APOE3 recovered from the inhibitory phase to the basal state faster than APOE4, neither of the APOE isoforms activated translation at a later time point (20 min) like NMDAR stimulation. Thus, the primary difference was the distinct temporal profiles of translation on APOE treatment and NMDAR stimulation, highlighting the specificity of the protein synthesis response downstream of synaptic stimulation.

We have previously shown that the inhibitory phase of the NMDAR translation response involved the translation activation of a specific subset of mRNAs like PTEN and PSD95 (Kute et al., 2019). Accordingly, APOE4 treatment (but not APOE3 treatment) caused the translation activation of PTEN and PSD95. Thus, APOE4 treatment mimicked the early phase NMDAR translation response, but as a consequence rendered the neurons non-responsive to physiological NMDAR stimulation. However, APOE3 treatment did not affect the protein synthesis response to NMDAR stimulation. Another interesting finding was that NMDAR stimulation in the presence of APOE4 led to a stress response phenotype by causing an inhibition of translation initiation and eIF2α phosphorylation. Thus, activity-mediated protein synthesis, which is salient in shaping synaptic plasticity, was impaired in APOE4-treated neurons; implying that the disruption of synaptic signaling is an important player in APOE4 pathology.

The specificity of the signal generated downstream of NMDARs is linked to their feature of high calcium permeability (Papadia and Hardingham, 2007; Lau et al., 2009; Higley and Sabatini, 2012). Previous studies have outlined the contribution of calcium in causing the inhibitory phase of NMDAR translation response (Scheetz et al., 2000; Ghosh Dastidar et al., 2020). Stimulation of NMDARs leads to a robust increase in intracellular calcium contributed by different sources such as NMDARs, L-VGCCs, and internal calcium stores; and their activation is regulated spatially and sequentially (Emptage et al., 1999; Higley and Sabatini, 2012; Griffith et al., 2016; Lee et al., 2016; Dittmer et al., 2017; Hiester et al., 2017). NMDARs lead to the first burst of calcium which further activates L-VGCCs, followed by internal stores through calcium-induced calcium release (CICR; Emptage et al., 1999; Lee et al., 2016; Dittmer et al., 2017; Hiester et al., 2017). Calcium being one of the most important secondary messengers, many kinases and phosphatases are sensitive to calcium (Colbran, 2004; Higley and Sabatini, 2012), and directly influence the signaling pathways that regulate protein synthesis (Higley and Sabatini, 2012). Thus, we hypothesized that the distinct translation responses generated downstream of synaptic stimulation could be a result of the specific calcium signatures. Hence, we explored the link between protein synthesis response and calcium homeostasis in the presence of APOE isoforms as a possible explanation for APOE4-mediated synaptic translation defects.

APOE was previously reported to cause an influx of calcium in neurons which has been linked to the activation of NMDARs (Tolar et al., 1999; Veinbergs et al., 2002; Qiu et al., 2003; Hoe et al., 2005; Xu and Peng, 2017). Thus, we assessed the calcium signatures generated by APOE3 and APOE4 and identified the calcium sources involved. APOE3 led to a small burst of calcium where the source of calcium was NMDARs. However, APOE4 caused a sustained increase in intracellular calcium where the contributing sources were both NMDARs and L-VGCCs. The NMDAR antagonist MK801 completely blocked the calcium influx caused by both APOE isoforms, further highlighting that NMDARs were the primary source of calcium entry. Consecutively, MK801 was also able to prevent the APOE3-mediated and APOE4-mediated translation inhibition at the early time point (1 min). APOE receptors and NMDARs are known to interact with each other (Bacskai et al., 2000; Hoe et al., 2005; Nakajima et al., 2013), specifically through the Dab1-SFK pathway (Hoe et al., 2005). Activation of the ERK signaling pathway by APOE is also shown to be dependent on NMDAR activation (Ohkubo et al., 2001; Qiu et al., 2004; Hoe et al., 2005). Although the influence of APOE receptor-associated signaling on NMDARs has been studied (Lane-Donovan and Herz, 2017), the exact mechanism behind APOE-mediated calcium influx through NMDARs is yet to be understood. Interestingly even in the presence of MK801, eEF2 phosphorylation still showed a trend of increase (although not statistically significant) in APOE4-treated neurons. Hence, although NMDAR calcium seems to be the primary initiating cause, we cannot rule out the possibility that other signaling pathways and NMDAR calcium independent mechanisms could be involved in APOE4-mediated increase in eEF2 phosphorylation.

Apart from the involvement of NMDARs, our results highlight the importance of L-VGCCs in sustaining the calcium increase on APOE4 treatment. L-VGCC antagonist nifedipine did not block the initial calcium entry on APOE4 treatment, but blocked its sustenance, further supporting the idea of sequential calcium entry where NMDARs were the first source and L-VGCCs were the latter. However, it is important to note that the initial NMDAR calcium component was also higher in the case of APOE4 compared with APOE3. The higher calcium influx through NMDARs could be the plausible explanation for the L-VGCC activation by APOE4 only. Additionally, there could be a possibility of APOE4 directly regulating the activation of L-VGCCs, hence causing the sustained increase of calcium. Corresponding to the calcium profile, nifedipine could not prevent the APOE4-mediated translation inhibition at the earlier time point (1 min), while it successfully rescued it at the later time point (20 min). These results support the idea that calcium signatures generated by the sequential activation of different sources generate distinct translation responses.

It is important to note that our model system (cultured cortical neurons) lacks the APOE clearance mechanisms which exist

physiologically. Thus, we speculate that many of the phenotypes we observe might be exaggerated and would probably be subtle in the brain. Previous studies have reported the effects of APOE4 on transcription, especially that of PSD95 mRNA (Huang et al., 2019). We did not observe any changes in the steady-state levels of PSD95 mRNA in our system.

With all the above points in consideration, we propose the model (Fig. 9) where we try to explain the calcium and translation signatures downstream of NMDAR stimulation and APOE treatment. NMDAR stimulation leads to calcium influx through NMDARs and L-VGCCs leading to its distinct translation response of early phase inhibition (corresponding to increased eEF2 phosphorylation) followed by a later phase activation (corresponding to decreased eEF2 phosphorylation; Fig. 9*A*). APOE3 causes a short burst of calcium through NMDARs alone, causing an early phase translation inhibition that recovers to the basal level. Hence, APOE3 treatment followed by NMDAR stimulation does not affect the NMDA-mediated translation response (Fig. 9*B*). APOE4 causes a robust and sustained influx of calcium through NMDARs and L-VGCCs. This leads to a sustained translation inhibition phase which recovers much slower than APOE3. APOE4-mediated regulation of L-VGCCs or other signaling pathways could also contribute to the sustained calcium and translation inhibition. Hence, in the background of APOE4 treatment, NMDAR stimulation leads to a stress response causing further reduction of protein synthesis (Fig. 9*C*).

Thus, our work identifies the translation defect caused by APOE4 and links it to the calcium signature generated by it. Additionally, it puts forth a new perspective toward protein synthesis regulation brought about by the distinct calcium signatures and their sources. Many studies are attempting to elucidate how APOE4 could cause AD phenotype independent of classical familial mutations of AD (Huang et al., 2017; Lin et al., 2018). We propose that protein synthesis dysregulation could be a central component responsible for synaptic and cognitive defects in APOE4-mediated pathology.

References

Ahmad F, Singh K, Das D, Gowaikar R, Shaw E, Ramachandran A, Rupanagudi KV, Kommaddi RP, Bennett DA, Ravindranath V (2017) Reactive oxygen species-mediated loss of synaptic Akt1 signaling leads to deficient activity-dependent protein translation early in Alzheimer's disease. Antioxid Redox Signal 27:1269–1280.

An WL, Cowburn RF, Li L, Braak H, Alafuzoff I, Iqbal K, Iqbal IG, Winblad B, Pei JJ (2003) Up-regulation of phosphorylated/activated p70 S6 kinase and its relationship to neurofibrillary pathology in Alzheimer's disease. Am J Pathol 163:591–607.

Bacskai BJ, Xia MQ, Strickland DK, Rebeck GW, Hyman BT (2000) The endocytic receptor protein LRP also mediates neuronal calcium signaling via N-methyl-D-aspartate receptors. Proc Natl Acad Sci USA 97:11551–11556.

Beckelman BC, Day S, Zhou X, Donohue M, Gouras GK, Klann E, Keene CD, Ma T (2016) Dysregulation of elongation factor 1A expression is correlated with synaptic plasticity impairments in Alzheimer's disease. J Alzheimers Dis 54:669–678.

Cefaliello C, Penna E, Barbato C, Di Ruberto G, Mollica MP, Trinchese G, Cigliano L, Borsello T, Chun JT, Giuditta A, Perrone-Capano C, Miniaci MC, Crispino M (2020) Deregulated local protein synthesis in the brain synaptosomes of a mouse model for Alzheimer's disease. Mol Neurobiol 57:1529–1541.

Chen Y, Durakoglugil MS, Xian X, Herz J (2010) ApoE4 reduces glutamate receptor function and synaptic plasticity by selectively impairing ApoE receptor recycling. Proc Natl Acad Sci USA 107:12011–12016.

Colbran RJ (2004) Protein phosphatases and calcium/calmodulin-dependent protein kinase II-dependent synaptic plasticity. J Neurosci 24:8404–8409.

De Jager PL, Shulman JM, Chibnik LB, Keenan BT, Raj T, Wilson RS, Yu L, Leurgans SE, Tran D, Aubin C, Anderson CD, Biffi A, Corneveaux JJ, Huentelman MJ; Alzheimer's Disease Neuroimaging Initiative, Rosand J, Daly MJ, Myers AJ, Reiman EM, Bennett DA, et al. (2012) A genome-wide scan for common variants affecting the rate of age-related cognitive decline. Neurobiol Aging 33:1017.e1–15.

Ding Q, Markesbery WR, Chen Q, Li F, Keller JN (2005) Ribosome dysfunction is an early event in Alzheimer's disease. J Neurosci 25:9171–9175.

Ding Q, Markesbery WR, Cecarini V, Keller JN (2006) Decreased RNA, and increased RNA oxidation, in ribosomes from early Alzheimer's disease. Neurochem Res 31:705–710.

Dittmer PJ, Wild AR, Dell'Acqua ML, Sather WA (2017) STIM1 Ca2+ sensor control of L-type Ca^{2+}-channel-dependent dendritic spine structural plasticity and nuclear signaling. Cell Rep 19:321–334.

Dumanis SB, Tesoriero JA, Babus LW, Nguyen MT, Trotter JH, Ladu MJ, Weeber EJ, Turner RS, Xu B, Rebeck GW, Hoe HS (2009) ApoE4 decreases spine density and dendritic complexity in cortical neurons in vivo. J Neurosci 29:15317–15322.

Elder MK, Erdjument-Bromage H, Oliveira HM, Mamcarz M, Neubert TA, Klann E (2020) Dysregulation of the *de novo* proteome accompanies pathology progression in the APP/PS1 mouse model of Alzheimer's disease. bioRxiv 260786.

Elder MK, Erdjument-Bromage H, Oliveira MM, Mamcarz M, Neubert TA, Klann E (2021) Age-dependent shift in the de novo proteome accompanies pathogenesis in an Alzheimer's disease mouse model. Commun Biol 4:823.

Emptage N, Bliss TVP, Fine A (1999) Single synaptic events evoke NMDA receptor-mediated release of calcium from internal stores in hippocampal dendritic spines. Neuron 22:115–124.

Evans HT, Benetatos J, van Roijen M, Bodea L-G, Götz J (2019) Decreased synthesis of ribosomal proteins in tauopathy revealed by non-canonical amino acid labelling. EMBO J 38:e101174.

Ghosh Dastidar S, Das Sharma S, Chakraborty S, Chattarji S, Bhattacharya A, Muddashetty RS (2020) Distinct regulation of bioenergetics and translation by group I mGluR and NMDAR. EMBO Rep 21:e48037.

Griffith T, Tsaneva-Atanasova K, Mellor JR (2016) Control of Ca^{2+} influx and calmodulin activation by SK-channels in dendritic spines. PLoS Comput Biol 12:e1004949.

Hardy J (2006) A hundred years of Alzheimer's disease research. Neuron 52:3–13.

Heise C, Gardoni F, Culotta L, di Luca M, Verpelli C, Sala C (2014) Elongation factor-2 phosphorylation in dendrites and the regulation of dendritic mRNA translation in neurons. Front Cell Neurosci 8:35.

Hernández-Ortega K, Garcia-Esparcia P, Gil L, Lucas JJ, Ferrer I (2016) Altered machinery of protein synthesis in Alzheimer's: from the nucleolus to the ribosome. Brain Pathol 26:593–605.

Hiester BG, Bourke AM, Sinnen BL, Cook SG, Gibson ES, Smith KR, Kennedy MJ (2017) L-type voltage-gated Ca^{2+} channels regulate synaptic-activity-triggered recycling endosome fusion in neuronal dendrites. Cell Rep 21:2134–2146.

Higley MJ, Sabatini BL (2012) Calcium signaling in dendritic spines. Cold Spring Harb Perspect Biol 4:a005686.

Hoe HS, Harris DC, Rebeck GW (2005) Multiple pathways of apolipoprotein E signaling in primary neurons. J Neurochem 93:145–155.

Hoeffer CA, Klann E (2008) NMDA receptors and translational control. In: Biology of the NMDA receptor (Van Dongen AM, ed). Boca Raton: CRC Press/Taylor & Francis.

Huang YWA, Zhou B, Wernig M, Südhof TC (2017) ApoE2, ApoE3, and ApoE4 differentially stimulate APP transcription and Aβ secretion. Cell 168:427–441.e21.

Huang YWA, Zhou B, Nabet AM, Wernig M, Südhof TC (2019) Differential signaling mediated by ApoE2, ApoE3, and ApoE4 in human neurons parallels Alzheimer's disease risk. J Neurosci 39:7408–7427.

Hunt DL, Castillo PE (2012) Synaptic plasticity of NMDA receptors: mechanisms and functional implications. Curr Opin Neurobiol 22:496–508.

Jiang C, Schuman EM (2002) Regulation and function of local protein synthesis in neuronal dendrites. Trends Biochem Sci 27:506–513.

Kelleher RJ, Govindarajan A, Tonegawa S (2004) Translational regulatory mechanisms in persistent forms of synaptic plasticity. Neuron 44:59–73.

Kim J, Basak JM, Holtzman DM (2009) The role of apolipoprotein E in Alzheimer's disease. Neuron 63:287–303.

Koren SA, Hamm MJ, Meier SE, Weiss BE, Nation GK, Chishti EA, Arango JP, Chen J, Zhu H, Blalock EM, Abisambra JF (2019) Tau drives translational selectivity by interacting with ribosomal proteins. Acta Neuropathol 137:571–583.

Kute PM, Ramakrishna S, Neelagandan N, Chattarji S, Muddashetty RS (2019) NMDAR mediated translation at the synapse is regulated by MOV10 and FMRP. Mol Brain 12:65.

Kuzniewska B, Cysewski D, Wasilewski M, Sakowska P, Milek J, Kulinski TM, Winiarski M, Kozielewicz P, Knapska E, Dadlez M, Chacinska A, Dziembowski A, Dziembowska M (2020) Mitochondrial protein biogenesis in the synapse is supported by local translation. EMBO Rep 21: e48882.

Lane-Donovan C, Herz J (2017) ApoE, ApoE receptors, and the synapse in Alzheimer's disease. Trends Endocrinol Metab 28:273–284.

Lau CG, Takeuchi K, Rodenas-Ruano A, Takayasu Y, Murphy J, Bennett MVL, Zukin RS (2009) Regulation of NMDA receptor Ca2+ signalling and synaptic plasticity. Biochem Soc Trans 37:1369–1374.

Lee KFH, Soares C, Thivierge JP, Béïque JC (2016) Correlated synaptic inputs drive dendritic calcium amplification and cooperative plasticity during clustered synapse development. Neuron 89:784–799.

Li X, An WL, Alafuzoff I, Soininen H, Winblad B, Pei JJ (2004) Phosphorylated eukaryotic translation factor 4E is elevated in Alzheimer brain. Neuroreport 15:2237–2240.

Lin YT, Seo J, Gao F, Feldman HM, Wen HL, Penney J, Cam HP, Gjoneska E, Raja WK, Cheng J, Rueda R, Kritskiy O, Abdurrob F, Peng Z, Milo B, Yu CJ, Elmsaouri S, Dey D, Ko T, Yankner BA, et al. (2018) APOE4 causes widespread molecular and cellular alterations associated with Alzheimer's disease phenotypes in human iPSC-derived brain cell types. Neuron 98:1141–1154.e7.

Liu CC, Liu CC, Kanekiyo T, Xu H, Bu G (2013) Apolipoprotein e and Alzheimer disease: risk, mechanisms and therapy. Nat Rev Neurol 9:106–118.

Liu DA, Pan XD, Zhang J, Shen H, Collins NC, Cole AM, Koster KP, Ben Aissa M, Dai XM, Zhou M, Tai LM, Zhu Y-g, LaDu M, Chen XC (2015) APOE4 enhances age-dependent decline in cognitive function by down-regulating an NMDA receptor pathway in EFAD-Tg mice. Mol Neurodegener 10:7–17.

Ma T, Hoeffer CA, Capetillo-Zarate E, Yu F, Wong H, Lin MT, Tampellini D, Klann E, Blitzer RD, Gouras GK (2010) Dysregulation of the mTOR pathway mediates impairment of synaptic plasticity in a mouse model of Alzheimer's disease. PLoS One 5:e12845.

Ma T, Trinh MA, Wexler AJ, Bourbon C, Gatti E, Pierre P, Cavener DR, Klann E (2013) Suppression of eIF2α kinases alleviates Alzheimer's disease-related plasticity and memory deficits. Nat Neurosci 16:1299–1305.

Matsuzaki M, Honkura N, Ellis-Davies GCR, Kasai H (2004) Structural basis of long-term potentiation in single dendritic spines. Nature 429:761–766.

May P, Rohlmann A, Bock HH, Zurhove K, Marth JD, Schomburg ED, Noebels JL, Beffert U, Sweatt JD, Weeber EJ, Herz J (2004) Neuronal LRP1 functionally associates with postsynaptic proteins and is required for normal motor function in mice. Mol Cell Biol 24:8872–8883.

Meier S, Bell M, Lyons DN, Rodriguez-Rivera J, Ingram A, Fontaine SN, Mechas E, Chen J, Wolozin B, LeVine H, Zhu H, Abisambra JF (2016) Pathological tau promotes neuronal damage by impairing ribosomal function and decreasing protein synthesis. J Neurosci 36:1001–1007.

Moreno JA, Halliday M, Molloy C, Radford H, Verity N, Axten JM, Ortori CA, Willis AE, Fischer PM, Barrett DA, Mallucci GR (2013) Oral treatment targeting the unfolded protein response prevents neurodegeneration and clinical disease in prion-infected mice. Sci Transl Med 5:206ra138.

Muddashetty RS, Kelić S, Gross C, Xu M, Bassell GJ (2007) Dysregulated metabotropic glutamate receptor-dependent translation of AMPA receptor and postsynaptic density-95 mRNAs at synapses in a mouse model of fragile X syndrome. J Neurosci 27:5338–5348.

Nakajima C, Kulik A, Frotscher M, Herz J, Schäfer M, Bock HH, May P (2013) Low density lipoprotein receptor-related protein 1 (LRP1) modulates N-methyl-D-aspartate (NMDA) receptor-dependent intracellular signaling and NMDA-induced regulation of postsynaptic protein complexes. J Biol Chem 288:21909–21923.

Nathan BP, Bellosta S, Sanan DA, Weisgraber KH, Mahley RW, Pitas RE (1994) Differential effects of apolipoproteins E3 and E4 on neuronal growth in vitro. Science 264:850–852.

Ohkubo N, Mitsuda N, Tamatani M, Yamaguchi A, Lee YD, Ogihara T, Vitek MP, Tohyama M (2001) Apolipoprotein E4 stimulates cAMP response element-binding protein transcriptional activity through the extracellular signal-regulated kinase pathway. J Biol Chem 276:3046–3053.

Pakos-Zebrucka K, Koryga I, Mnich K, Ljujic M, Samali A, Gorman AM (2016) The integrated stress response. EMBO Rep 17:1374–1395.

Papadia S, Hardingham GE (2007) The dichotomy of NMDA receptor signaling. Neuroscientist 13:572–579.

Paul A, Nawalpuri B, Shah D, Sateesh S, Muddashetty RS, Clement JP (2019) Differential regulation of syngap1 translation by FMRP modulates eEF2 mediated response on NMDAR activity. Front Mol Neurosci 12:97.

Piedrahita JA, Zhang SH, Hagaman JR, Oliver PM, Maeda N (1992) Generation of mice carrying a mutant apolipoprotein E gene inactivated by gene targeting in embryonic stem cells. Proc Natl Acad Sci USA 89:4471–4475.

Qiu Z, Crutcher KA, Hyman BT, Rebeck GW (2003) apoE isoforms affect neuronal N-methyl-D-aspartate calcium responses and toxicity via receptor-mediated processes. Neuroscience 122:291–303.

Qiu Z, Hyman BT, Rebeck GW (2004) Apolipoprotein E receptors mediate neurite outgrowth through activation of p44/42 mitogen-activated protein kinase in primary neurons. J Biol Chem 279:34948–34956.

Radford H, Moreno JA, Verity N, Halliday M, Mallucci GR (2015) PERK inhibition prevents tau-mediated neurodegeneration in a mouse model of frontotemporal dementia. Acta Neuropathol 130:633–642.

Ravindran S, Nalavadi VC, Muddashetty RS (2019) BDNF induced translation of limk1 in developing neurons regulates dendrite growth by fine-tuning cofilin1 activity. Front Mol Neurosci 12:64.

Reas ET, Laughlin GA, Bergstrom J, Kritz-Silverstein D, Barrett-Connor E, McEvoy LK (2019) Effects of APOE on cognitive aging in community-dwelling older adults. Neuropsychology 33:406–416.

Richter JD, Klann E (2009) Making synaptic plasticity and memory last: mechanisms of translational regulation. Genes Dev 23:1–11.

Rodriguez GA, Burns MP, Weeber EJ, Rebeck GW (2013) Young APOE4 targeted replacement mice exhibit poor spatial learning and memory, with reduced dendritic spine density in the medial entorhinal cortex. Learn Mem 20:256–266.

Scheetz AJ, Nairn AC, Constantine-Paton M (2000) NMDA receptor-mediated control of protein synthesis at developing synapses. Nat Neurosci 3:211–216.

Schmid B, Prehn KR, Nimsanor N, Garcia BIA, Poulsen U, Jørring I, Rasmussen MA, Clausen C, Mau-Holzmann UA, Ramakrishna S, Muddashetty R, Steeg R, Bruce K, Mackintosh P, Ebneth A, Holst B, Cabrera-Socorro A (2019) Generation of a set of isogenic, gene-edited iPSC lines homozygous for all main APOE variants and an APOE knockout line. Stem Cell Res 34:101349.

Shankar GM, Walsh DM (2009) Alzheimer's disease: synaptic dysfunction and Abeta. Mol Neurodegener 4:48.

Sheng Z, Prorok M, Brown BE, Castellino FJ (2008) N-methyl-d-aspartate receptor inhibition by an apolipoprotein E-derived peptide relies on low-density lipoprotein receptor-associated protein. Neuropharmacology 55:204–214.

Shi Y, Kirwan P, Livesey FJ (2012) Directed differentiation of human pluripotent stem cells to cerebral cortex neurons and neural networks. Nat Protoc 7:1836–1846.

Small BJ, Rosnick CB, Fratiglioni L, Bäckman L (2004) Apolipoprotein E and cognitive performance: a meta-analysis. Psychol Aging 19:592–600.

Sutton MA, Schuman EM (2006) Dendritic protein synthesis, synaptic plasticity, and memory. Cell 127:49–58.

Suzanne Zukin R, Richter JD, Bagni C (2009) Signals, synapses, and synthesis: how new proteins control plasticity. Front Neural Circuits 3:14.

Takahashi RH, Almeida CG, Kearney PF, Yu F, Lin MT, Milner TA, Gouras GK (2004) Oligomerization of Alzheimer's β-amyloid within processes and synapses of cultured neurons and brain. J Neurosci 24:3592–3599.

Tanzi RE (2012) The genetics of Alzheimer disease. Cold Spring Harb Perspect Med 2:a006296.

Teter B, Xu PT, Gilbert JR, Roses AD, Galasko D, Cole GM (2002) Defective neuronal sprouting by human apolipoprotein E4 is a gain-of-negative function. J Neurosci Res 68:331–336.

Tolar M, Keller JN, Chan S, Mattson MP, Marques MA, Crutcher KA (1999) Truncated apolipoprotein E (ApoE) causes increased intracellular calcium and may mediate ApoE neurotoxicity. J Neurosci 19:7100–7110.

Tom Dieck S, Müller A, Nehring A, Hinz FI, Bartnik I, Schuman EM, Dieterich DC (2012) Metabolic labeling with noncanonical amino acids and visualization by chemoselective fluorescent tagging. Curr Protoc Cell Biol Chapter 7:Unit 7.11.

Ulrich JD, Burchett JM, Restivo JL, Schuler DR, Verghese PB, Mahan TE, Landreth GE, Castellano JM, Jiang H, Cirrito JR, Holtzman DM (2013) In vivo measurement of apolipoprotein e from the brain interstitial fluid using microdialysis. Mol Neurodegener 8:13.

Veinbergs I, Everson A, Sagara Y, Masliah E (2002) Neurotoxic effects of apolipoprotein E4 are mediated via dysregulation of calcium homeostasis. J Neurosci Res 67:379–387.

Wang C, Wilson WA, Moore SD, Mace BE, Maeda N, Schmechel DE, Sullivan PM (2005) Human apoE4-targeted replacement mice display synaptic deficits in the absence of neuropathology. Neurobiol Dis 18:390–398.

Wang C, Najm R, Xu Q, Jeong D-E, Walker D, Balestra ME, Yoon SY, Yuan H, Li G, Miller ZA, Miller BL, Malloy MJ, Huang Y (2018) Gain of toxic apolipoprotein E4 effects in human iPSC-derived neurons is ameliorated by a small-molecule structure corrector article. Nat Med 24:647–657.

Wisdom NM, Callahan JL, Hawkins KA (2011) The effects of apolipoprotein E on non-impaired cognitive functioning: a meta-analysis. Neurobiol Aging 32:63–74.

Xu D, Peng Y (2017) Apolipoprotein E 4 triggers multiple pathway-mediated Ca2+ overload, causes CaMK II phosphorylation abnormity and aggravates oxidative stress caused cerebral cortical neuron damage. Eur Rev Med Pharmacol Sci 21:5717–5728.

Yang W, Zhou X, Zimmermann HR, Cavener DR, Klann E, Ma T (2016) Repression of the eIF2α kinase PERK alleviates mGluR-LTD impairments in a mouse model of Alzheimer's disease. Neurobiol Aging 41:19–24.

Yong SM, Lim ML, Low CM, Wong BS (2014) Reduced neuronal signaling in the ageing apolipoprotein-E4 targeted replacement female mice. Sci Rep 4:6580.

Zhang Y, Schmid B, Nikolaisen NK, Rasmussen MA, Aldana BI, Agger M, Calloe K, Stummann TC, Larsen HM, Nielsen TT, Huang J, Xu F, Liu X, Bolund L, Meyer M, Bak LK, Waagepetersen HS, Luo Y, Nielsen JE, Holst B, et al. (2017) Patient iPSC-derived neurons for disease modeling of frontotemporal dementia with mutation in CHMP2B. Stem Cell Reports 8:648–658.